New Cocrystallization Method: Non-photochemical Laser-Induced Nucleation of a Cocrystal of Caffeine–Gallic Acid in Water

Dania Mellah, Béatrice Nicolaï, Bertrand Fournier, Nada Bošnjaković-Pavlović, Francois-Xavier Legrand, Pascale Gemeiner, Vincent Boemare, Nicolas Guiblin, Ali Assi, Ali Tfayli, et al.

A new cocrystallization method: Non-Photochemical Laser-Induced Nucleation (NPLIN) of a cocrystal of caffeine–gallic acid in water

Dania MELLAH[1,2], Béatrice NICOLAÏ[1,3], Bertrand FOURNIER[1,2], Nada BOŠNJAKOVIĆ-PAVLOVIĆ[1], Francois-Xavier LEGRAND[2], Pascale GEMEINER[1], Vincent BOEMARE[1], Nicolas GUIBLIN[1], Ali ASSI[4], Ali TFAYLI[4], Sokona KONATE[5], Pierrick DURAND[6], Anne SPASOJEVIĆ-DE BIRÉ[1*]

[1] Université Paris-Saclay, CentraleSupélec, CNRS, Laboratoire SPMS, 91190, Gif-sur-Yvette, France.

[2] Université Paris-Saclay, CNRS, Institut Galien Paris-Saclay, 92296, Châtenay-Malabry, France.

[3] Faculté de Pharmacie, Université Paris-Cité, 75006 Paris, France.

[4] Université Paris-Saclay, Lipides : systèmes analytiques et biologiques, EA7357, 92296, Châtenay-Malabry, France.

[5] Université Paris-Saclay, CentraleSupélec, ENS Paris-Saclay, CNRS, LMPS - Laboratoire de Mécanique Paris-Saclay, 91190, Gif-sur-Yvette, France.

[6] Laboratoire de Cristallographie, Résonance Magnétique et Modélisations (CRM2) UMR 7036 CNRS, Université de Lorraine, Boulevard des Aiguillettes, 54506 Vandoeuvre-Lès-Nancy Cedex, France.

To be submitted to CG&D

* to whom correspondence should be addressed

Abstract

This paper reports for the first time the crystallization of cocrystals (caffeine - gallic acid) in water using the Non-Photochemical Laser-Induced Nucleation (NPLIN) technique. The nucleation temporal control of NPLIN and the induction time reduction (70 times shorter than spontaneous nucleation) allow the obtention of cocrystals *on-demand*, with excellent repeatability. Prior to NPLIN experiments, solubility measurements, metastable zone limit determination, and spontaneous nucleation (SN) are carried out. Supersaturated solutions at three different molarities of caffeine (0.0158, 0.0167 and 0.0179 M) are prepared and dissolved at 338 K. Supersaturated solutions are exposed to a 532 nm wavelength nanosecond pulsed laser at 296 K. Some hours later crystals can be filtered. The impact of supersaturation on probability of nucleation has been studied and the result shows a higher supersaturation implies a higher probability of nucleation. Crystalline form characterization has employed a combination of Raman scattering, high-performance liquid chromatography, thermogravimetry, differential scanning calorimetry, and powder X-ray diffraction; the sizes of the cocrystals being too small for a single-crystal X-ray diffraction experiment. Two different cocrystal forms are obtained: a new polymorph of hemihydrate **CAFGAL.0.5H$_2$O** from spontaneous nucleation by precipitation, and a new hydrate form **CAFGAL.1.5H$_2$O** from NPLIN and from spontaneous nucleation of a supersaturated solution without evaporation. These results open a promising way to crystallize cocrystals in the context of the pharmaceutical industry.

I. Introduction

Non-Photochemical Laser-Induced Nucleation (NPLIN) is a nucleation method that uses, as an external field, a laser. This technique discovered accidentally by Garetz et al [1] allowed the crystallization of urea from a supersaturated aqueous solution using a laser beam at 1,064 nm. This method was then taken up by various laboratories and has grown rapidly in recent years, with some variations on the setup / laser. However, depending on the authors, different names to the experiment were given, leading to different abbreviations (NPLIN [1], laser irradiation [2], LIGHT [3], laser-induced crystallization [4], optical breakdown [5], photon pressure [6], LIN (Laser-Induced Nucleation) [7], laser trapping crystallization [8], optical trapping [9], laser-induced cavitation [10], laser shock wave induced crystallization [11], light induced crystallization [12], LIPS [13], LIPSaN [14], ...) often referring to a putative mechanism. For a better understanding of this method and thus to contribute to the broadening of its use, Clair et al [15] extended the definition of NPLIN to any nucleation experiment of a supersaturated solution crystallizing after being illuminated by a laser beam. Alexander and Camp [16] limit the use of the NPLIN terms to the nucleation of supersaturated solutions or supercooled melts using unfocused millijoule nanosecond laser pulses. Sugiyama and Wang [17] in a very recent paper have compiled all the experiments included in the Clair et al definition under the term *laser-induced nucleation*. In this paper, we will use the abbreviation NPLIN, for all the laser-induced nucleation experiments, while their putative mechanism should be different depending, for example, on the laser type. According to this definition, all these published works correspond to almost 100 papers, up to now [18]. NPLIN has been applied to small organic species [1,19] as well as proteins [3,19] or inorganic compounds [20,21]. Primary nucleation is stochastic by nature so in general, it is not possible to control the time, location, and morphology of the new phase crystallizing. All these NPLIN works have demonstrated a shortening of the nucleation induction time from some days to some seconds, minutes, or hours depending on the compounds and the detection

technique. Thus, NPLIN implies a temporal control of the nucleation. In the cases of focused laser experiments, NPLIN enables a spatial control of the nucleation (see for example [22]). A polymorphism control can also occur, depending on the laser polarization (linear or circular) (see for example [23]). Moreover, the crystalline state (powder, multi-crystal, or single crystal) can be controlled (see for example [24]). NPLIN technique is a complex phenomenon and there is still debate about the possible mechanisms involved [16,17]. However, to the best of our knowledge, NPLIN has never led to a new crystalline structure (polymorphs or hydrates).

80% of Active Pharmaceutical Ingredients (API) are commercialized in solid forms (crystalline or amorphous phase) [25]. A lot of these API's are small organic molecules. A proper selection of the solid form in which an API is used for drug formulation can be decisive. The formulation depends indeed on the physicochemical properties of the solid form. When an API has different polymorphic forms, working with the more stable one avoids crystal phase transition during manufacturing or storage. However, this polymorph may have unsatisfactory properties, especially solubility, hence bioavailability [26]. In order to improve the API's physicochemical properties without impairing its pharmaceutical properties, the API can be crystallized with another molecule called "coformer". This approach is referred to as "cocrystallization" and has been given special attention from pharmaceutical industries during these last years [27]. The coformers are usually chosen for their innocuousness in the GRAS list (« Generally Recognized As Safe » molecules), the coformer can also be another API. Cocrystals present different physicochemical properties than the pure API: solubility in water may be increased, stability can be enhanced, susceptibility to moisture can be reduced, and so forth. [28]

Several APIs have been crystallized *via* NPLIN: L-histidine [29], acetaminophen [30], carbamazepine [31], indomethacin [32], sulfathiazole [33,34] and aspirin [35]. However, no nucleation *via* NPLIN has been tried in the specific case of the co-crystals.

The goal of this paper is to demonstrate that it is possible to induce with a laser the cocrystallization of an API with its coformer. The selected API is the caffeine (CAF) because it is a reference molecule in the cocrystallization field: numerous cocrystals have been reported in the CSD (Cambridge Structural Database), in addition to its three polymorphic and hydrate forms. The aim of a CAF cocrystal is to decrease the sensitivity to moisture. More than thirty cocrystals have been reported between CAF and carboxylic acids. Among them, one can mention oxalic acid, [36] malonic acid, [36] maleic acid, [36] glutaric acid, [36] formic acid, [37] acetic acid, [37] trifluoroacetic acid, [37] citric acid, [38] succinic acid, [39] 2-, 3-, 4-hydroxybenzoic- and 2,3-, 2,4-, 2,5-, 3,4-, and 3,5-dihydroxybenzoic acid, [40] gallic acid, [41,44] 2-hydroxy-1-naphthoic acid, [45] p-coumaric acid, [46] 4-hydroxybenzoic acid, [47] benzoic acid, [48] p-formylphenoxyacetic acid, [49] 1- and 2-naphthoxyacetic acid, [50] dipicolinic acid, [51] 4-chloro-3-nitrobenzoic acid, [52] cinnamic acid, [53] mesaconic acid, [54] dimethylsuccinic acid, [54] L-malic acid, [54] anthranilic acid, [55] 5-aminoisophthalic acid, [56] 3-nitrobenzoic acid, [57] tannic acid, [42] glycolic acid, [58] trimesic acid, [59] isophthalic acid, [59] benzene-1,3,5-tricarboxylic, [60] benzene-1,2,3-tricarboxylic acid, [60]. In some cases, CAF is used in a drug-drug cocrystal such as with saccharin, [61] quercetin, [62] eosin, [53] theophylline, [63] sulfacetamide, [64] furosemide, [65] genistein, [66] myricetin, [67] dihydromyricetin, [68] 4-aminosalicylic acid, [69] baicalein, [70] epalrestat, [71] indomethacin, [72] paracetamol, [73] zonisamide, [74] dapsone, [75] 5-fluorocytosine, [76] luteolin, [77] naringenin, [78] fisetin, [79] famotidine, [80] hydrochlorothiazide, [81] apixaban, [82] pyrimethamine, [83] niflumic acid, [84] and chlorthalidone. [85]

The criteria to select the coformer for an NPLIN experiment could be described as follows: a molecule i) that has a great facility to crystallize attested by many structures reported; ii) that its solubility is close to that of CAF in the given solvent; iii) that does not absorb at 532 nm. Among them, gallic acid (GAL) has been chosen, in this NPLIN study. Its aqueous solubility is relatively close to the one of CAF. [86,87] GAL exhibits three polymorphic forms and several hydrates, cocrystals, or salts [89]. Spontaneous nucleation and laser-induced nucleation of CAF and GAL in water are reported in this paper. Clarke et al [41] have crystallized and characterized by single X-ray diffraction a cocrystal of formula **CAFGAL.0.5H$_2$O**. Dabir et al. [43] have

studied its thermodynamical properties, while Syed et al [42] have studied its stability. The crystals obtained are observed by optical microscopy and characterized by differential scanning calorimetry (DSC), thermogravimetry (TG), Raman spectroscopy, high-performance liquid chromatography (HPLC), and powder X-ray diffraction (PXRD).

II. Materials and methods

The internal names of the compounds are named as follows: CAF-GAL_X_T, where X represents the cocrystallization method or the name of the first author if it concerns a compound of the literature, and T the temperature of the measurements (110 for a single X-ray diffraction performed at 110 K) or the temperature of the oven (353 K for example). These internal names will be used in the text until the characterization methods allow us to use a chemical formula such as CAF-GAL.xH_2O where x represents the number of water molecules. This information is summarized in scheme 1.

II.1. Materials

Commercial white powders of CAF (≥ 99.0 %) and GAL (≥ 97.5 %) have been purchased from Sigma-Aldrich. Their crystalline forms have been identified by PXRD and DSC measurements. Commercial CAF corresponds to the polymorphic form II, which transforms into form I around 423 K, melting at 523 K (Figures S1). Commercial GAL corresponds to the polymorphic form II which melts around 537 K (Figures S2).

II.2. Spontaneous cocrystallization by precipitation

118 mg of CAF is entirely dissolved in 6 mL of distilled water at room temperature. 106 mg of GAL is progressively added at room temperature. The initial concentrations of CAF and GAL are close to their respective saturations at the experimental temperature 296 K. A white powder

precipitates rapidly and is filtered with a sintered glass filter. In order to compare with the cocrystal of Syed et al, [42] a part of the obtained powder is dried in an oven at 353 K for a minimum of 24 hours. The powder obtained by spontaneous nucleation (SN) is referred to as CAF-GAL_SN_A_296 and its dried fraction to as CAF-GAL_SN_A_353.

II.3. High-performance liquid chromatography (HPLC)

The stoichiometry and the solubility of the products were determined by HPLC.

An excess of solid powder (either CAF, GAL, CAF-GAL_SN_A_296) is added to distilled water. The samples are left for at least three days in a thermostatically controlled room at 296 K. Precautions are taken that some undissolved solid remained in the solution at equilibrium, to guarantee the solution saturation. An amount of saturated solution of CAF, GAL or cocrystal (CAF-GAL_SN_A_296) is withdrawn at 296 K, filtered with a syringe MILLEX- GV (porosity 0.22 µm), diluted with distilled water, and then analyzed by HPLC. CAF and GAL concentrations were determined using a Thermo Scientific UltiMate 3000 UHPLC system equipped with SRD-3600 solvent degasser, DGP-3600RS dual-gradient pump, WPS-3000TSL autosampler, TCC-3000 thermostated column compartment and DAD-3000 Diode Array Detector. A C18 chromatographic column (Agilent Zorbax Eclipse Plus C18, 3.5 µm, 4.6 × 100 mm) thermostated at 298 K was used for separation. The mobile phase was comprised of a mixture of water, acetonitrile, and formic acid (90:9:0.4, v/v/v). The flow rate was set at 0.5 mL/min, and the injection volume at 10 µL. A linear calibration curve was prepared using CAF in water at concentrations between 100 µg/mL and 1100 µg/mL at a wavelength of 273 nm. In the case of GAL, a non-linear calibration curve was obtained with the same conditions (solvent, range of concentration, analysis wavelength).

II.4. Non-Photochemical Laser-Induced Nucleation (NPLIN) experiments

The experimental laser-induced nucleation set-up has been previously described [15] (see SI, section S1). The laser Continuum 8010 Powerlite with a wavelength of 532 nm is used, the beam diameter of 9 mm is reduced to 3.5 mm using a long focal lens (Figure S3).

The temperature and time profile of the metastable solution production and the NPLIN experiment has been schematized (Figure S4). 50 mL of an aqueous solution of CAF and GAL with three different molarities of 0.0158 M, 0.0167 M, and 0.0179 M in respect to CAF and GAL have been prepared and dissolved in an ultrasound bath at 338 K (Table S1). When the powder is fully dissolved, 1 mL of the hot solution is transferred to standard HPLC tubes of 1.5 mL carefully closed in order to avoid evaporation and left for a few hours (3 to 12 hours) in the carousel at 338 K. Temperature is then slowly decreased to the experiment temperature (cooling time of 5 hours to reach 296 K). An aging time from 3 to 15 hours has been decided to allow the formation of aggregates in the solutions, thus increasing the probability of nucleation after laser irradiation. The laser exposure is done vertically on HPLC tubes closed by a glass disc associated with a seal to prevent evaporation. However, the need for such step in an NPLIN experiment is still upon the discussion in the literature [90] Due to the stochastic nature of the nucleation, a significant number of tubes has been prepared. The numbers of tubes prepared, exposed to the laser, and where crystals have been observed are reported in Table S1. The power above the tube is 0.4 $GW.cm^{-2}$ and the exposure time 10 s corresponding to 100 pulses. Cocrystal obtained *via* NPLIN is referred to as CAF-GAL_NPLIN_296. The product is dried in an oven at 353 K for a minimum of 24 hours, analyzed and referred to as CAF-GAL_NPLIN_353.

Some tubes have not been exposed to laser allowing us to determine the metastable zone limit. Crystals obtained in such experiences are analyzed and referred to as CAF-GAL_SN_B_296.

II.5 Raman spectroscopy

Raman scattering spectra of initial products and of the obtained cocrystals are recorded with a spectrometer T64000 from HORIBA Jobin Yvon, characterized by excitation radiation at 488 nm and a nitrogen-cooled CCD detector. This spectrometer is set in a triple subtractive configuration for low frequency measurements, with a focal length of 640 mm and a resolution of 0.6 cm^{-1}. These spectra are used as references for the Raman attribution. For each nucleation experiment, all the crystals obtained are identified by their Raman spectra recorded on a second spectrophotometer Labram from HORIBA Jobin Yvon (excitation radiation at 633 nm).

II.6 Powder X-Ray Diffraction (PXRD) experiments and refinements

PXRD is performed on a Bruker D2 Phaser in reflection mode using Bragg-Brentano geometry. This diffractometer is equipped with a XFlash detector using Copper (Kα1 = 1.54061 Å) radiation. Samples are ground in order to avoid preferential orientations and are placed on a Plexiglas sample holder.

PXRD temperature investigations are done on a high-resolution prototype goniometer [91] with seven axis. The goniometer is equipped with a 18 kW Rigaku UltraX18 rotating anode operating at 50 kV and 200 mA. A graphite monochromator for CuK_α radiation (λ = 1.5406 Å) is used. The XRPD measurements are performed in the temperature range 300–520 K using a Rigaku furnace with temperature stability better than 0.7 K. All the samples are carefully ground in order to avoid preferential orientations.

DICVOL06 [92] software, implemented in the FULLPROF suite, [92] is used to index experimental powder patterns. The lattice parameters were then refined using the Le Bail refinement method available in FULLPROF.

II.7 Differential scanning calorimetry (DSC) and thermogravimetric (TG) measurements

DSC is performed with a DSC 220C (SEIKO) calibrated with indium (T_{fusion} = 429.75 K, ΔH_{fusion} = 3267 J.mol^{-1}) and aluminum crucibles are used. The heating rate is set at 5 K.min^{-1} over a range from 296 K to 677 K. Specimens are weighted with a balance sensitive to 0.02 mg. TG measurements are carried out with a TG/DSC 92 (SETARAM) equipped with an S-type oven thermocouple and S-type TG/DSC rod. The heating rate is 5 K.min^{-1}. A DSC spectrum is performed after the TG experiment in order to confirm the temperature values.

III. Results and discussion

III.1. Preliminary results

In order to control an NPLIN experiment for cocrystallization, different preliminary experiments have to be performed i) determination of the solubility of the CAF, GAL and CAF-GAL_SN_A_296 in the given solvent; ii) determination of the metastable zone limit (MZL) in order to prove than the nucleation is laser-induced. For doing that, spontaneous nucleation must be realized in almost the same conditions as the NPLIN experiment.

CAF-GAL_SN_A_296 crystals are observed by microscope and appear as very small needles glued in aggregates (Figure 1f). Unfortunately, they are too small and cannot be manipulated and separated for a full crystalline structure determination with a conventional single-crystal X-ray diffractometer. However, CAF-GAL_SN_A_296 is characterized by different techniques (*vide infra*).

III.1.1 Solubility of crystals obtained by spontaneous crystallization

Three saturated solutions are obtained with an excess solid (CAF, GAL and CAF-GAL_SN_A_296) in distilled water. The concentration of the saturated solution has been

determined by HPLC in duplicate. The average solubility values are S_0(CAF) = 0.083(4) mol/L and S_0(GAL) = 0.045(4) mol/L.

The measured solubility of the cocrystal is S_0(CAF-GAL_SN_A_296) = 0.0085(3) mol/L. The solubility values found for CAF and CAF-GAL_SN_A_296 are in relatively good agreement with the values reported by Dabir et al. [43] and Shalmashi et al. [86] (S_0(CAF-GAL_Dabir_303) = 0.0119 mol/L at 303 K [43]) whereas the value for pure GAL is slightly smaller than the ones found by Dabir et al. [43] (Figures S5a, b). The solids obtained during the solubility measurements are analyzed with PXRD. CAF hydrate has been obtained in the saturated CAF solution, GAL mono hydrate form I [88] has been obtained in the saturated GAL solution, and CAF-GAL_SN_A_296 in the saturated CAF-GAL_SN_A_296 solution.

III.1.2 Metastable zone limit determination

100 samples-holders, filled with three different molarities, are submitted to the same protocol described above. The crystallization process is followed by optical microscopy each hour (at the bottom and at the meniscus of the tube). Thus, the spontaneous nucleation induction time is t_{ind} (0.0158 M) = 15 days, t_{ind} (0.0167 M) = 12 days and t_{ind} (0.0179 M) = 9 days. These values determine the metastable zone limit. That means that if an aging time is less than t_{ind}, the nucleation event is due to the laser. It is important to notice that it is true only if no evaporation occurs in the meantime. Nucleation site of those crystals obtained spontaneously in closed vials is the meniscus. The obtained crystals are dried at 353 K for 24 hours. Those crystals referred to as a CAF-GAL_SN_B_296 and CAF-GAL_SN_B_353 are characterized by DSC and Raman spectroscopy (*vide infra*).

III.2. NPLIN experiments

Cocrystal obtained *via* NPLIN, is referred to as CAF-GAL_NPLIN_296 (Figure 1). The tubes are filtered when the crystals are visible with a microscope, generally after around 24 to 36 hours, this is far below the nucleation time without the laser (the induction time being 9 days minimum). The nucleation site of CAF-GAL_NPLIN_296 is the meniscus (Figure 1a) as well as the one observed for CAF-GAL_SN_B_296. The crystals CAF-GAL_NPLIN_296 appear always as very fine needles (3-4 μm width, 250 μm length) (Figure 1d). When those needles are filtered, they tend to form agglomerates (Figure 1e).

Probability of nucleation is defined as the ratio of the number of tubes in which crystals have been observed with the number of exposed tubes. It is illustrated in Figure 2 and presents a classical behavior: a higher molarities implies a higher probability of nucleation. [15,29,31] Due to the very slow crystallization kinetics, probability of nucleation has been reported on the day of the experiment and two days after, while the shortest MZL limit is nine days. Filtration is done when the tiny crystals are detectable at the meniscus by human eyes and therefore suitable for Raman analysis (see Figure 1e for an estimation of the size of the agglomerates after filtration). Within these experiments (MZL determination and pictures of the laser-induced nucleation crystals), it is indisputable that the laser induces the nucleation of crystals.

Compared to other organic compounds studied *via* NPLIN in the same experimental setup, the crystalline growth speed of the cocrystal is so far lower. For glycine [15], carbamazepine [31] and sulfathiazole, [33] the induction time is between 10 to 30 minutes and filtered after only 3 hours, while the MZL limit varies from 1.5 to 7 days for glycine [15], 3 days for carbamazepine [31] and 7 days for sulfathiazole [33]. In these three cases, MZL is lower than those observed with CAF-GAL cocrystals, crystallization kinetics is slower by a factor ten, and the size of the cocrystal is very small.

The crucial point is now the identification of the crystals. The size of the latter is too small to allow a single-crystal X-ray diffraction determination, therefore careful identification with other techniques is necessary.

III.3. Characterization

III.3.1. Determination of the molecular components involved in the cocrystal by Raman spectroscopy

The first technique used is the Raman scattering because it determines if the crystals contain both molecules (CAF and GAL) and could discriminate between different polymorphs. Additionally, there is no published work on cocrystals of CAF and GAL characterized by Raman spectroscopy. Table S2 contains the attribution of the Raman spectra as reported in the literature by Edwards et al, [93] Pompeu et al [94] and Mohammed-Ziegler [95] for the initial products, as well as the spectra recorded in this work (CAF hydrate, anhydrous CAF form II, GAL form II, CAF-GAL_SN_A_296, CAF-GAL_SN_A_353, CAF-GAL_NPLIN_296, CAF-GAL_NPLIN_353, CAF-GAL_SN_B_296, and CAF-GAL_SN_B_353). The spectra (Figure 3) of the two wet crystals (CAF hydrate and CAF-GAL_SN_A_296) exhibit low Raman intensities leading only to a few peaks detectable. However, the dried crystals give spectra with a good accuracy allowing a precise characterization.

A close inspection of the spectra in the lattice vibration mode zone of the four compounds CAF-GAL_SN_A_296, CAF-GAL_NPLIN_296 is done and demonstrates unambiguously that these crystals cannot be assigned to a mixture of CAF hydrate or anhydrous CAF and GAL (Figure 3a insert).

The stretching frequencies $\nu_{C=CH}$(CAF-GAL_NPLIN_296) = 3139 cm^{-1} and ν_{CH3}(CAF-GAL_NPLIN_296) = 2958 cm^{-1}. These frequencies are characteristic of CAF molecule and do not exist in GAL molecule. In the region around 960 cm^{-1}, a strong peak is observed for GAL

which can be attributed to the deformation of the benzene ring Def-R(GAL) = 961 cm^{-1} while Def-R (CAF-GAL_SN_A_296) = 958 cm^{-1}, Def-R (CAF-GAL_SN__A_353) = 958 cm^{-1}, Def-R (CAF-GAL_NPLIN_296) = 953 cm^{-1} and Def-R (CAF-GAL_NPLIN_353) = 958 cm^{-1}. There is no peak of CAF in that region coherent with the attribution. [93] Therefore, one can unambiguously state that the four crystals obtained in this work contain at least one GAL molecule.

Many peaks are also characteristics of the CAF molecule. For example, in the region around 650 cm^{-1}, the $\delta_{OC(N)} + \delta_{pyrimidine\ imidazole\ ring)}$ (CAF) = 643 cm^{-1} while $\delta_{CH(N)}$ (CAF-GAL_SN__A_353) = 655 cm^{-1} and $\delta_{CH(N)}$ (CAF-GAL_NPLIN_296) = 653 cm^{-1}.

At very low vibration mode, the peak positions are different (Figure 3b) when comparing CAF-GAL_SN_A_296 and CAF_SN_A_353 (presence of a peak at 19 cm^{-1} only in the form at high temperature). A similar observation is made for CAF-GAL_NPLIN_296 and CAF_NPLIN_353 (presence of a peak at 19 cm^{-1} only in the form at high temperature). That indicates that the two forms (CAF-GAL_SN_A_296 and CAF-GAL_NPLIN_296) transform at high temperature in a same crystalline form.

Finally, the crystals obtained spontaneously when measuring the metastable zone limit (CAF-GAL_SN_B_296) and those obtained by laser-induced nucleation (CAF-GAL_NPLIN_296) have the same Raman spectra. Therefore, they present the same crystalline form.

Consequently, the Raman spectroscopy indicates that: i) CAF-GAL_SN_A_296, CAF-GAL_SN_B_296, CAF-GAL_SN_A_353, CAF-GAL_NPLIN_296, and CAF-GAL_NPLIN_353 are cocrystals of CAF and GAL; ii) there is a crystallographic transformation between CAF-GAL_SN_A_296 and CAF-GAL_SN_A_353 (and also between CAF-GAL_NPLIN_296 and CAF-GAL_NPLIN_353); iii) CAF-GAL_SN_A_353 and CAF-GAL_NPLIN_353 seem to be similar but it is not the case with CAF-GAL_SN_A_296 and CAF-GAL_NPLIN_296; iv) CAF-GAL_SN_B_296 is very similar to CAF-GAL_NPLIN_296

(Figure 3b), whereas CAF-GAL_SN_B_353 is similar to CAF-GAL_SN_A_353 and CAF-GAL_NPLIN_353.

The results show that at that step, the stoichiometry remains unknown.

III.3.2. Determination of stoichiometry and the hydrate composition by HPLC and TG

In the preliminary experiment to determine the solubility of CAF-GAL_SN_A_296 at 296 K, an excess powder was added to distilled water, in order to have an equilibrium between the solid and the saturated solution. The mixture has been left for three days at 296 K, and the saturated solution is filtered and analyzed by HPLC twice. Concentrations are 0.00876(6) mol/L for CAF and 0.00833(6) mol/L for GAL on average. The ratio of these two concentrations is 1.05. This means that the CAF-GAL_SN_A_296 powder has a 1:1 stoichiometry. The solubility can then be described by the solubility product K_S [96] as: $K_s = [CAF] \times [GAL]$ where $[CAF]$ and $[GAL]$ are the solution concentrations of caffeine and gallic acid respectively. $S = [CAF] = [GAL]$ (in mol/L) is the solution concentration of caffeine or gallic acid at saturation. Thus, $K_s = S^2$, and K_s(CAF-GAL_SN_A_296) = 7.3(5) × 10^{-5}.

A TG/DSC measurement of the CAF-GAL_SN_A_296 powder reveals a mass loss of 2.4 % around 356 K (Table 1, Figure 4b), meaning that the initial cocrystal contains 0.5 moles of water for 1 mole of CAF and 1 mole of GAL. No further mass loss was observed until the complete decomposition of the solid around 513 K. Consequently, CAF-GAL_SN_A_296 is a CAF:GAL (1:1) hemihydrate with a formula of **CAFGAL.0.5H_2O** whereas CAF-GAL_SN_A_353 is the anhydrous form of this cocrystal (Table 1, Figure 4a).

Due to technical reasons, it has not been possible to determine the solubility of CAF-GAL_NPLIN_296, but the stoichiometry by HPLC for CAF-GAL_NPLIN_296 has been determined with a value of 1.07(9). Therefore, a 1:1 stoichiometry for CAF-GAL_NPLIN_296 could be reasonably considered.

A TG measurement of the CAF-GAL_NPLIN_296 powder reveals a mass loss of 7.9 % around 316.5 K (Table 1, Figure 5c), meaning that the initial cocrystal contains 1.5 moles of water for 1 mole of CAF and 1 mole of GAL. No further mass loss was observed until the complete decomposition of the solid around 513 K. Consequently, the cocrystal is a CAF:GAL (1:1) sesquihydrate. Its composition can be described as **CAFGAL.1.5H_2O** whereas CAF-GAL_NPLIN_353 is an anhydrous form identical to the anhydrous form CAF-GAL_SN_A_353.

III.3.3. Cocrystal polymorphism determined by PXRD and DSC

PXRD diffractograms are recorded at room temperature on CAF-GAL_SN_A_296, CAF-GAL_SN_A_353, CAF-GAL_NPLIN_296, and CAF-GAL_NPLIN_353 (Figure 5), and compared to those published in the literature by Clarke et al. [41] Dabir et al**.** [43] and Syed et al. [42]

The diffractogram of CAF-GAL_SN_A_296 and CAF-GAL_NPLIN_296 are different. At low angle ($2\Theta < 12°$) CAF-GAL_SN_A_296 and CAF-GAL_NPLIN_296 exhibit two fine peaks at different positions. Around ($2\Theta = 26°$) there is no peak for CAF-GAL_SN_A_296 while CAF-GAL_NPLIN_296 presents a sharp peak. When an absence of a diffraction peak is noticed, it could be due to a preferential orientation inhibiting the diffraction of some plane. This could be plausible because the cocrystals are very anisotropic needles. However, this hypothesis is ruled out for two reasons: i) the Raman spectra have already stated that the two cocrystals have two different structures ii) samples have been carefully ground.

PXRD diffractograms (Figure 4) indicate that the anhydrous forms in the literature and in this work are very similar, thus CAF-GAL_SN_A_353 = CAF-GAL_NPLIN_353 = CAF-GAL_Clarke_373 = CAF-GAL_Dabir_373.

Clarke et al. [41] have reported the single-crystal structure at 100 K of a CAF-GAL cocrystal referred to as MUPNOB refcode in CSD. The chemical formula of CAF-GAL_Clarke_100 is **CAFGAL.0.5H$_2$O** with a reported mass loss of 1.9% around 373 K and a melting point of 515K. The authors have recorded the PXRD diffractogram of the dried crystals (dried in an oven at 373K), the chemical formula is, therefore, **CAFGAL.0H$_2$O**. CAF-GAL_SN_A_296 has also the chemical formula **CAFGAL.0.5H$_2$O**. Therefore, the question which arises is the following: does CAF-GAL_SN_A_296 have the same structure as CAF-GAL_Clarke_100 or is it a polymorphic form of **CAFGAL.0.5H$_2$O**? This question will be definitively addressed below with the DSC measurements, however, the calculated pattern of Clarke at 100 K seems different to the experimental pattern of CAF-GAL_SN_A_296.

It is important to notice that the spontaneous crystallization process of this work is very different to the one of Clarke et al. [41] (they obtained their cocrystal from a slow evaporation of a methanol solution at room temperature) and it is relatively similar to the process of Dabir et al. [43] and Syed et al. [42] (the main difference is that they dissolved separately CAF and GAL in distilled water, whereas a unique solution close to the saturation of the two compounds is used in this work). Clarke et al. [41] have prepared the cocrystal by slow evaporation in methanol. That means that only a small amount of water (coming from the solvent or the humidity of the air) has contributed to the crystallization. The powder pattern of CAF-GAL_SN_A_296 and CAF-GAL_SN_A_353 are successfully indexed with DICVOL06, [92] and a Le Bail refinement was performed with FULLPROF program [16] (Figures S6 and S7 and Table 2). The volume is significantly smaller than that of CAF-GAL_Clarke_100 because of water loss (1405*2=2810 > 2343 Å^3).

TG/DSC experiments were performed on CAF-GAL_SN_A_296, CAF-GAL_SN_A_353, CAF-GAL_NPLIN_296. The main results are summarized in Table 1, and the original curves are compiled in Figure 5. The following observations can be drawn. i) cocrystals obtained by

spontaneous coprecipitation and by NPLIN present transition temperatures significatively different than those observed by Clarke et al. [41] (343 K, for CAF-GAL_SN_A_296, 317.5 K for CAF-GAL_NPLIN_296, while for CAF-GAL_Clarke_296 the transition temperature is 409 K); ii) the melting points for the co-crystals obtained in this work are lower than those already reported in the literature [41,43]; iii) there is a second event observed on the CAF-GAL_SN_A_296 cocrystals close to the melting point of the NPLIN cocrystals; iv) At the end of the experiment, a residual black matter stays in the aluminum pan and the mass was considerably reduced. From these observations, one can make the following hypothesis: i) CAF-GAL_SN_A_296, which has already been characterized as **CAFGAL.0.5H$_2$O**, is the polymorph of CAF-GAL_Clarke_296 = MUPNOB reported by Clarke *et al*. [41] Therefore CAF-GAL_Clarke_100 can now be labelled as **CAFGAL.0.5H$_2$O form I** and CAF-GAL_SN_A_296 should be labelled as **CAFGAL.0.5H$_2$O form II**.

PXRD diffractograms studied as a function of temperature in the range 295 - 510 K for CAF-GAL_SN_A_296 and CAF-GAL_NPLIN_296 powders are presented in Figure 6. The estimated transition temperature has been reported in Table 2. The difference between the transition temperatures may be due to the difference in the temperature ramp in the DSC and the PXRD experiments. In the PXRD experiments, the powder has time to reach an equilibrium at each step. Moreover, the sesquihydrate does not transform to the hemihydrate form I or form II. All the compounds - i.e. the two new forms discover in this work (**CAFGAL.0.5H$_2$O form II** and **CAFGAL.1.5H$_2$O**) and the already published one (**CAFGAL.0.5H$_2$O form I**) - transform to the same cocrystal (**CAFGAL.0H$_2$O**) (Figure 6c).

IV. Conclusion

The different characterizations lead to:

CAF-GAL_SN_A_296 = **CAFGAL.0.5H$_2$O** form II

CAF-GAL_NPLIN_296 = CAF-GAL_SN_B_296 = **CAFGAL.1.5H$_2$O**

CAF-GAL_SN_ A_353 = **CAFGAL.0H$_2$O =** CAF-GAL_Clarke_373

CAF-GAL_NPLIN_353 = **CAFGAL.0H$_2$O =** CAF-GAL_Clarke_373

CAF-GAL_SN_ A_353 = CAF-GAL_NPLIN_353 = CAF-GAL_SN_B_353

CAFGAL.0.5H$_2$O form II $\xrightarrow{\Delta}$ **CAFGAL.0H$_2$O**

CAFGAL.1.5H$_2$O $\xrightarrow{\Delta}$ **CAFGAL.0H$_2$O**

while CAF-GAL_Clarke_353 = **CAFGAL.0.5H$_2$O** form I

This work has, therefore, allowed the discovery of two new cocrystals of CAF and GAL: one being a polymorph of the already reported phase obtained by spontaneous nucleation precipitation (**CAFGAL.0.5H$_2$O** form II), the second discovered *via* NPLIN and its MZL determination (**CAFGAL.1.5H$_2$O**).

In conclusion, using a laser-induced nucleation method (NPLIN), a cocrystal of CAF and GAL has been crystallized. This is important because it gives a new tool for cocrystallization in the pharmaceutical context. In the case of similar solubilities of the two components of the cocrystal, and after mastering the preparation of supersaturation solution in a given solvent at the desired temperature, the NPLIN method sounds as a very useful method. With its temporal control of nucleation and its reduction of induction time properties, one can obtain cocrystals *on-demand*, with excellent repeatability. Furthermore, thanks to the high polymorphic character of the API and its coformer, two new crystalline forms were characterized in this work. Consequently, NPLIN method demonstrates its power: it can also be used to obtain cocrystals. Moreover, this work clearly indicates that the laser has dramatically reduced the induction time (a factor of 70 has been observed for the highest supersaturation).

The characterization of these two crystalline forms was difficult due to the fact that the cocrystals were needles too small for single-crystal X-ray diffraction. Further investigations are necessary and are actually developed in four directions: i) developing a methodology to obtain cocrystals *on-demand* based on their ternary diagram of this system; ii) realizing a parametric sweep on the NPLIN experiments such as the impact of the laser intensity, the exposition duration, the laser polarization, the pulse duration, the nucleation site on the probability of nucleation as well as the polymorphic form. These works will give new insight in the mechanism; iii) obtaining a single-crystal structure of the new polymorphic form using the synchrotron radiation; iv) expanding the system to other solvent and coformers.

V. Supporting Information. Section S1. Experimental NPLIN set-up description. **Table S1**. Solution preparation for NPLIN experiment. **Table S2.** Raman spectra attribution as reported in the literature for the initial products, as well as the spectra recorded in this work. **Figure S1.** PXRD and DSC spectra identification of CAF. **Figure S2.** PXRD spectra identification of GAL. **Figure S3.** Experimental NPLIN set-up. **Figure S4.** Temperature / time process for supersaturated solution preparation. **Figure S5.** HPLC solubility curves of a) CAF, b) GAL and c) CAF-GAL_SN_A_296. **Figure S6.** Observed, calculated and difference in the cell refinement of PXRD of CAF-GAL_SN_A_296 b) CAF-GAL_SN_A_353. **Figure S7.** Observed, calculated and difference in the cell refinement of PXRD of CAF-GAL_SN_A_353. **Figure S8.** DSC curves for cocrystals.

V. References

(1) Garetz, B.; Aber, J.; Goddard, N.; Young, R.; Myerson, A. Nonphotochemical, Polarization-Dependent, Laser-Induced Nucleation in Supersaturated Aqueous Urea Solutions. *Phys. Rev. Lett.* **1996**, *77* (16), 3475. https://doi.org/10.1103/PhysRevLett.77.3475.

(2) Tsunesada, F.; Iwai, T.; Watanabe, T.; Adachi, H.; Yoshimura, M.; Mori, Y.; Sasaki, T. High-Quality Crystal Growth of Organic Nonlinear Optical Crystal DAST. *J. Cryst. Growth* **2002**, *237–239*, 2104–2106. https://doi.org/10.1016/S0022-0248(01)02266-7.

(3) Adachi, H.; Takano, K.; Hosokawa, Y.; Inoue, T.; Mori, Y.; Matsumura, H.; Yoshimura, M.; Tsunaka, Y.; Morikawa, M.; Kanaya, S.; Masuhara, H.; Kai, Y.; Sasaki, T. Laser Irradiated Growth of Protein Crystal. *Jpn. J. Appl. Phys.* **2003**, *42* (Part 2, No. 7B), 798–800. https://doi.org/10.1143/JJAP.42.L798.

(4) Hosokawa, Y.; Adachi, H.; Yoshimura, M.; Mori, Y.; Sasaki, T.; Masuhara, H. Femtosecond Laser-Induced Crystallization of 4-(Dimethylamino)- *N* -Methyl-4-Stilbazolium Tosylate. *Cryst. Growth Des.* **2005**, *5* (3), 861–863. https://doi.org/10.1021/cg049709y.

(5) Lindinger, B.; Mettin, R.; Chow, R.; Lauterborn, W. Ice Crystallization Induced by Optical Breakdown. *Phys. Rev. Lett.* **2007**, *99* (4), 045701. https://doi.org/10.1103/PhysRevLett.99.045701.

(6) Sugiyama, T.; Adachi, T.; Masuhara, H. Crystallization of Glycine by Photon Pressure of a Focused CW Laser Beam. *Chem. Lett.* **2007**, *36* (12), 1480–1481. https://doi.org/10.1246/cl.2007.1480.

(7) Yoshikawa, H. Y.; Murai, R.; Maki, S.; Kitatani, T.; Sugiyama, S.; Sazaki, G.; Adachi, H.; Inoue, T.; Matsumura, H.; Takano, K.; Murakami, S.; Sasaki, T.; Mori, Y. Laser Energy Dependence on Femtosecond Laser-Induced Nucleation of Protein. *Appl. Phys. A* **2008**, *93* (4), 911–915. https://doi.org/10.1007/s00339-008-4790-x.

(8) Rungsimanon, T.; Yuyama, K.; Sugiyama, T.; Masuhara, H. Crystallization in Unsaturated Glycine/D_2O Solution Achieved by Irradiating a Focused Continuous Wave Near Infrared Laser. *Cryst. Growth Des.* **2010**, *10* (11), 4686–4688. https://doi.org/10.1021/cg100830x.

(9) Tsuboi, Y.; Shoji, T.; Kitamura, N. Optical Trapping of Amino Acids in Aqueous Solutions. *J. Phys. Chem. C* **2010**, *114* (12), 5589–5593. https://doi.org/10.1021/jp9072334.

(10) Soare, A.; Dijkink, R.; Pascual, M. R.; Sun, C.; Cains, P. W.; Lohse, D.; Stankiewicz, A. I.; Kramer, H. J. M. Crystal Nucleation by Laser-Induced Cavitation. *Cryst. Growth Des.* **2011**, *11* (6), 2311–2316. https://doi.org/10.1021/cg2000014.

(11) Jacob, J. A.; Sorgues, S.; Dazzi, A.; Mostafavi, M.; Belloni, J. Homogeneous Nucleation-Growth Dynamics Induced by Single Laser Pulse in Supersaturated Solutions. *Cryst. Growth Des.* **2012**, *12* (12), 5980–5985. https://doi.org/10.1021/cg301024t.

(12) Shilpa, T. Small and Macromolecules Crystallization Induced by Focused Ultrafast Laser. *Proc. Indian Natl. Sci. Acad.* **2015**, *81* (2). https://doi.org/10.16943/ptinsa/2015/v81i2/48104.

(13) Walton, F.; Wynne, K. Control over Phase Separation and Nucleation Using a Laser-Tweezing Potential. *Nat. Chem.* **2018**, *10* (5), 506–510. https://doi.org/10.1038/s41557-018-0009-8.

(14) Walton, F.; Wynne, K. Using Optical Tweezing to Control Phase Separation and Nucleation near a Liquid–Liquid Critical Point. *Soft Matter* **2019**, *15* (41), 8279–8289. https://doi.org/10.1039/C9SM01297D.

(15) Clair, B.; Ikni, A.; Li, W.; Scouflaire, P.; Quemener, V.; Spasojević-de Biré, A. A New Experimental Setup for High-Throughput Controlled Non-Photochemical Laser-Induced Nucleation: Application to Glycine Crystallization. *J. Appl. Crystallogr.* **2014**, *47* (4), 1252–1260. https://doi.org/10.1107/S160057671401098X.

(16) Alexander, A. J.; Camp, P. J. Non-Photochemical Laser-Induced Nucleation. *J. Chem. Phys.* **2019**, *150* (4), 040901. https://doi.org/10.1063/1.5079328.

(17) Sugiyama, T.; Wang, S.-F. Manipulation of Nucleation and Polymorphism by Laser Irradiation. *J. Photochem. Photobiol. C Photochem. Rev.* **2022**, *52*, 100530. https://doi.org/10.1016/j.jphotochemrev.2022.100530.
(18) Wang, W.; Wang, S.; Sugiyama, T. L-serine Polymorphism Controlled by Optical Trapping with High-repetition-rate Femtosecond Laser Pulses. *J. Chin. Chem. Soc.* **2022**, *69* (1), 200–210. https://doi.org/10.1002/jccs.202100269.
(19) Yuyama, K.; Chang, K.-D.; Tu, J.-R.; Masuhara, H.; Sugiyama, T. Rapid Localized Crystallization of Lysozyme by Laser Trapping. *Phys. Chem. Chem. Phys.* **2018**, *20* (9), 6034–6039. https://doi.org/10.1039/C7CP06990A.
(20) Alexander, A. J.; Camp, P. J. Single Pulse, Single Crystal Laser-Induced Nucleation of Potassium Chloride. *Cryst. Growth Des.* **2009**, *9* (2), 958–963. https://doi.org/10.1021/cg8007415.
(21) Liu, Y.; Qiu, Q.; Ding, G.; You, W. Effect of Acidic Polymers on the Morphology of Laser-Induced Nucleation of Cesium Chloride. *ACS Omega* **2021**, *6* (4), 2699–2706. https://doi.org/10.1021/acsomega.0c04902.
(22) Liao, Z.; Wynne, K. A Metastable Amorphous Intermediate Is Responsible for Laser-Induced Nucleation of Glycine. *J. Am. Chem. Soc.* **2022**, *144* (15), 6727–6733. https://doi.org/10.1021/jacs.1c11154.
(23) Matic, J.; Sun, X.; Garetz, B. A.; Myerson, A. S. Intensity, Wavelength, and Polarization Dependence of Nonphotochemical Laser-Induced Nucleation in Supersaturated Aqueous Urea Solutions. *Cryst. Growth Des.* **2005**, *5* (4), 1565–1567. https://doi.org/10.1021/cg050041c.
(24) Liu, Y.; He, H.; Liu, Y. Morphology Control of Laser-Induced Dandelion-like Crystals of Sodium Acetate through the Addition of Acidic Polymers. *J. Appl. Crystallogr.* **2021**, *54* (4), 1111–1120. https://doi.org/10.1107/S1600576721005409.
(25) Ticehurst, M. D.; Marziano, I. Integration of Active Pharmaceutical Ingredient Solid Form Selection and Particle Engineering into Drug Product Design. *J. Pharm. Pharmacol.* **2015**, *67* (6), 782–802. https://doi.org/10.1111/jphp.12375.
(26) Lu, J.; Rohani, S. Polymorphism and Crystallization of Active Pharmaceutical Ingredients (APIs). *Curr. Med. Chem.* **2009**, *16* (7), 884–905. https://doi.org/10.2174/092986709787549299.
(27) Liu, L.; Wang, J.-R.; Mei, X. Enhancing the Stability of Active Pharmaceutical Ingredients by the Cocrystal Strategy. *CrystEngComm* **2022**, *24* (11), 2002–2022. https://doi.org/10.1039/D1CE01327K.
(28) Guo, M.; Sun, X.; Chen, J.; Cai, T. Pharmaceutical Cocrystals: A Review of Preparations, Physicochemical Properties and Applications. *Acta Pharm. Sin. B* **2021**, *11* (8), 2537–2564. https://doi.org/10.1016/j.apsb.2021.03.030.
(29) Sun, X.; Garetz, B. A.; Myerson, A. S. Polarization Switching of Crystal Structure in the Nonphotochemical Laser-Induced Nucleation of Supersaturated Aqueous L -Histidine. *Cryst. Growth Des.* **2008**, *8* (5), 1720–1722. https://doi.org/10.1021/cg800028v.
(30) Wang, S.; Wang, S.; Jiang, L.; Wang, M.; Wei, Y.; Sun, J.; Zhan, S.; Li, X.; Qu, L. Polymorph-Controlled Crystallization of Acetaminophen through Femtosecond Laser Irradiation. *Cryst. Growth Des.* **2019**, *19* (6), 3265–3271. https://doi.org/10.1021/acs.cgd.9b00123.
(31) Ikni, A.; Clair, B.; Scouflaire, P.; Veesler, S.; Gillet, J.-M.; El Hassan, N.; Dumas, F.; Spasojević-de Biré, A. Experimental Demonstration of the Carbamazepine Crystallization from Non-Photochemical Laser-Induced Nucleation in Acetonitrile and

Methanol. *Cryst. Growth Des.* **2014**, *14* (7), 3286–3299. https://doi.org/10.1021/cg500163c.
(32) Ikeda, K.; Maruyama, M.; Takahashi, Y.; Mori, Y.; Yoshikawa, H. Y.; Okada, S.; Adachi, H.; Sugiyama, S.; Takano, K.; Murakami, S.; Matsumura, H.; Inoue, T.; Yoshimura, M.; Mori, Y. Selective Crystallization of the Metastable Phase of Indomethacin at the Interface of Liquid/Air Bubble Induced by Femtosecond Laser Irradiation. *Appl. Phys. Express* **2015**, *8* (4), 045501. https://doi.org/10.7567/APEX.8.045501.
(33) Li, W.; Ikni, A.; Scouflaire, P.; Shi, X.; El Hassan, N.; Gémeiner, P.; Gillet, J.-M.; Spasojević-de Biré, A. Non-Photochemical Laser-Induced Nucleation of Sulfathiazole in a Water/Ethanol Mixture. *Cryst. Growth Des.* **2016**, *16* (5), 2514–2526. https://doi.org/10.1021/acs.cgd.5b01526.
(34) Yu, J.; Yan, J.; Jiang, L. Crystallization of Polymorphic Sulfathiazole Controlled by Femtosecond Laser-Induced Cavitation Bubbles. *Cryst. Growth Des.* **2021**, *21* (6), 3202–3210. https://doi.org/10.1021/acs.cgd.0c01476.
(35) Tsuri, Y.; Maruyama, M.; Fujimoto, R.; Okada, S.; Adachi, H.; Yoshikawa, H. Y.; Takano, K.; Murakami, S.; Matsumura, H.; Inoue, T.; Tsukamoto, K.; Imanishi, M.; Yoshimura, M.; Mori, Y. Crystallization of Aspirin Form II by Femtosecond Laser Irradiation. *Appl. Phys. Express* **2019**, *12* (1), 015507. https://doi.org/10.7567/1882-0786/aaf419.
(36) Trask, A. V.; Motherwell, W. D. S.; Jones, W. Pharmaceutical Cocrystallization: Engineering a Remedy for Caffeine Hydration. *Cryst. Growth Des.* **2005**, *5* (3), 1013–1021. https://doi.org/10.1021/cg0496540.
(37) Trask, A. V.; van de Streek, J.; Motherwell, W. D. S.; Jones, W. Achieving Polymorphic and Stoichiometric Diversity in Cocrystal Formation: Importance of Solid-State Grinding, Powder X-Ray Structure Determination, and Seeding. *Cryst. Growth Des.* **2005**, *5* (6), 2233–2241. https://doi.org/10.1021/cg0501682.
(38) Karki, S.; Friščić, T.; Jones, W.; Motherwell, W. D. S. Screening for Pharmaceutical Cocrystal Hydrates via Neat and Liquid-Assisted Grinding. *Mol. Pharm.* **2007**, *4* (3), 347–354. https://doi.org/10.1021/mp0700054.
(39) Friščić, T.; Trask, A. V.; Motherwell, W. D. S.; Jones, W. Guest-Directed Assembly of Caffeine and Succinic Acid into Topologically Different Heteromolecular Host Networks upon Grinding. *Cryst. Growth Des.* **2008**, *8* (5), 1605–1609. https://doi.org/10.1021/cg700929e.
(40) Bučar, D.-K.; Henry, R. F.; Lou, X.; Duerst, R. W.; MacGillivray, L. R.; Zhang, G. G. Z. Cocrystals of Caffeine and Hydroxybenzoic Acids Composed of Multiple Supramolecular Heterosynthons: Screening via Solution-Mediated Phase Transformation and Structural Characterization. *Cryst. Growth Des.* **2009**, *9* (4), 1932–1943. https://doi.org/10.1021/cg801178m.
(41) Clarke, H. D.; Arora, K. K.; Bass, H.; Kavuru, P.; Tien Teng Ong; Pujari, T.; Wojtas, L.; Zaworotko, M. J. Structure−Stability Relationships in Cocrystal Hydrates: Does the Promiscuity of Water Make Crystalline Hydrates the Nemesis of Crystal Engineering? *Cryst. Growth Des.* **2010**, *10* (5), 2152–2167. https://doi.org/10.1021/cg901345u.
(42) Syed, T. A.; Gaikar, V. G.; Mukherjee, S. Stability of Co-Crystals of Caffeine with Gallic Acid in Presence of Coformers. *J. Food Process Eng.* **2019**, *42* (4), e13066. https://doi.org/10.1111/jfpe.13066.
(43) Dabir, T.; Gaikar, V.; Jayaraman, S.; Mukherjee, S. Thermodynamic Modeling Studies of Aqueous Solubility of Caffeine, Gallic Acid and Their Cocrystal in the Temperature

Range of 303 K–363 K. *Fluid Phase Equilibria* **2017**, *456*. https://doi.org/10.1016/j.fluid.2017.09.021.
(44) Vella-Zarb, L.; Baisch, U. Crystal Water as the Molecular Glue for Obtaining Different Co-Crystal Ratios: The Case of Gallic Acid Tris-Caffeine Hexahydrate. *Acta Crystallogr. Sect. E Crystallogr. Commun.* **2018**, *74* (4), 559–562. https://doi.org/10.1107/S2056989018004528.
(45) Bučar, D.-K.; Henry, R. F.; Duerst, R. W.; Lou, X.; MacGillivray, L. R.; Zhang, G. G. Z. A 1:1 Cocrystal of Caffeine and 2-Hydroxy-1-Naphthoic Acid Obtained via a Slurry Screening Method. *J. Chem. Crystallogr.* **2010**, *40* (11), 933–939. https://doi.org/10.1007/s10870-010-9766-y.
(46) Schultheiss*, N.; Roe, M.; Boerrigter, S. X. M. Cocrystals of Nutraceuticalp-Coumaric Acid with Caffeine and Theophylline: Polymorphism and Solid-State Stability Explored in Detail Using Their Crystal Graphs. *CrystEngComm* **2011**, *13* (2), 611–619. https://doi.org/10.1039/C0CE00214C.
(47) Aitipamula, S.; Chow, P. S.; Tan, R. B. H. Co-Crystals of Caffeine and Piracetam with 4-Hydroxybenzoic Acid: Unravelling the Hidden Hydrates of 1 : 1 Co-Crystals. *CrystEngComm* **2012**, *14* (7), 2381. https://doi.org/10.1039/c2ce25080b.
(48) Bučar, D.-K.; Day, G. M.; Halasz, I.; Zhang, G. G. Z.; Sander, J. R. G.; Reid, D. G.; MacGillivray, L. R.; Duer, M. J.; Jones, W. The Curious Case of (Caffeine)·(Benzoic Acid): How Heteronuclear Seeding Allowed the Formation of an Elusive Cocrystal. *Chem. Sci.* **2013**, *4* (12), 4417. https://doi.org/10.1039/c3sc51419f.
(49) Suresh Kumar, G. S.; Seethalakshmi, P. G.; Bhuvanesh, N.; Kumaresan, S. Cocrystals of Caffeine with Formylphenoxyaliphatic Acids: Syntheses, Structural Characterization, and Biological Activity. *J. Mol. Struct.* **2013**, *1034*, 302–309. https://doi.org/10.1016/j.molstruc.2012.10.033.
(50) Suresh Kumar, G. S.; Seethalakshmi, P. G.; Sumathi, D.; Bhuvanesh, N.; Kumaresan, S. Syntheses, Structural Characterization, and DPPH Radical Scavenging Activity of Cocrystals of Caffeine with 1- and 2-Naphthoxyacetic Acids. *J. Mol. Struct.* **2013**, *1035*, 476–482. https://doi.org/10.1016/j.molstruc.2012.12.022.
(51) Moghimi, A.; Khavasi, H. R.; Dashtestani, F.; Kordestani, D.; Behboodi, E.; Maddah, B. A Cocrystal of Caffeine and Dipicolinic Acid: Synthesis, Characterization, X-Ray Crystallography, and Solution Studies. *J. Struct. Chem.* **2013**, *54* (5), 990–995. https://doi.org/10.1134/S0022476613050247.
(52) Ghosh, S.; Mondal, A.; Kiran, M. S. R. N.; Ramamurty, U.; Reddy, C. M. The Role of Weak Interactions in the Phase Transition and Distinct Mechanical Behavior of Two Structurally Similar Caffeine Co-Crystal Polymorphs Studied by Nanoindentation. *Cryst. Growth Des.* **2013**, *13* (10), 4435–4441. https://doi.org/10.1021/cg400928v.
(53) Suresh Kumar, G. S.; Seethalakshmi, P. G.; Bhuvanesh, N.; Kumaresan, S. Studies on the Syntheses, Structural Characterization, Antimicrobial-, and DPPH Radical Scavenging Activity of the Cocrystals Caffeine:Cinnamic Acid and Caffeine:Eosin Dihydrate. *J. Mol. Struct.* **2013**, *1050*, 88–96. https://doi.org/10.1016/j.molstruc.2013.07.018.
(54) Leyssens, T.; Tumanova, N.; Robeyns, K.; Candoni, N.; Veesler, S. Solution Cocrystallization, an Effective Tool to Explore the Variety of Cocrystal Systems: Caffeine/Dicarboxylic Acid Cocrystals. *CrystEngComm* **2014**, *16* (41), 9603–9611. https://doi.org/10.1039/C4CE01495B.

(55) Fischer, F.; Scholz, G.; Benemann, S.; Rademann, K.; Emmerling, F. Evaluation of the Formation Pathways of Cocrystal Polymorphs in Liquid-Assisted Syntheses. *CrystEngComm* **2014**, *16* (35), 8272–8278. https://doi.org/10.1039/C4CE00472H.
(56) Singh, M. P.; Tarai, A.; Baruah, J. B. Neutral, Zwitterion, Ionic Forms of 5-Aminoisophthalic Acid in Cocrystals, Salts and Their Optical Properties. *ChemistrySelect* **2019**, *4* (19), 5427–5436. https://doi.org/10.1002/slct.201901111.
(57) Singaraju, A. B.; Bahl, D.; Wang, C.; Swenson, D. C.; Sun, C. C.; Stevens, L. L. Molecular Interpretation of the Compaction Performance and Mechanical Properties of Caffeine Cocrystals: A Polymorphic Study. *Mol. Pharm.* **2020**, *17* (1), 21–31. https://doi.org/10.1021/acs.molpharmaceut.9b00377.
(58) Alvarez-Lorenzo, C.; Castiñeiras, A.; Frontera, A.; García-Santos, I.; González-Pérez, J. M.; Niclós-Gutiérrez, J.; Rodríguez-González, I.; Vílchez-Rodríguez, E.; Zaręba, J. K. Recurrent Motifs in Pharmaceutical Cocrystals Involving Glycolic Acid: X-Ray Characterization, Hirshfeld Surface Analysis and DFT Calculations. *CrystEngComm* **2020**, *22* (40), 6674–6689. https://doi.org/10.1039/D0CE01064B.
(59) Abosede, O. O.; Gordon, A. T.; Dembaremba, T. O.; Lorentino, C. M. A.; Frota, H. F.; Santos, A. L. S.; Hosten, E. C.; Ogunlaja, A. S. Trimesic Acid–Theophylline and Isopthalic Acid–Caffeine Cocrystals: Synthesis, Characterization, Solubility, Molecular Docking, and Antimicrobial Activity. *Cryst. Growth Des.* **2020**, *20* (5), 3510–3522. https://doi.org/10.1021/acs.cgd.0c00301.
(60) Gołdyn, M. R.; Larowska, D.; Bartoszak-Adamska, E. Novel Purine Alkaloid Cocrystals with Trimesic and Hemimellitic Acids as Coformers: Synthetic Approach and Supramolecular Analysis. *Cryst. Growth Des.* **2021**, *21* (1), 396–413. https://doi.org/10.1021/acs.cgd.0c01242.
(61) Padrela, L.; Rodrigues, M. A.; Velaga, S. P.; Fernandes, A. C.; Matos, H. A.; de Azevedo, E. G. Screening for Pharmaceutical Cocrystals Using the Supercritical Fluid Enhanced Atomization Process. *J. Supercrit. Fluids* **2010**, *53* (1–3), 156–164. https://doi.org/10.1016/j.supflu.2010.01.010.
(62) Smith, A. J.; Kavuru, P.; Wojtas, L.; Zaworotko, M. J.; Shytle, R. D. Cocrystals of Quercetin with Improved Solubility and Oral Bioavailability. *Mol. Pharm.* **2011**, *8* (5), 1867–1876. https://doi.org/10.1021/mp200209j.
(63) Eddleston, M. D.; Patel, B.; Day, G. M.; Jones, W. Cocrystallization by Freeze-Drying: Preparation of Novel Multicomponent Crystal Forms. *Cryst. Growth Des.* **2013**, *13* (10), 4599–4606. https://doi.org/10.1021/cg401179s.
(64) Rajesh Goud, N.; Khan, R. A.; Nangia, A. Modulating the Solubility of Sulfacetamide by Means of Cocrystals. *CrystEngComm* **2014**, *16* (26), 5859–5869. https://doi.org/10.1039/C4CE00103F.
(65) Pal, S.; Roopa, B. N.; Abu, K.; Manjunath, S. G.; Nambiar, S. Thermal Studies of Furosemide–Caffeine Binary System That Forms a Cocrystal. *J. Therm. Anal. Calorim.* **2014**, *115* (3), 2261–2268. https://doi.org/10.1007/s10973-013-3031-5.
(66) Sowa, M.; Ślepokura, K.; Matczak-Jon, E. Solid-State Characterization and Solubility of a Genistein–Caffeine Cocrystal. *J. Mol. Struct.* **2014**, *1076*, 80–88. https://doi.org/10.1016/j.molstruc.2014.07.036.
(67) Bazylińska, U.; Pucek, A.; Sowa, M.; Matczak-Jon, E.; Wilk, K. A. Engineering of Phosphatidylcholine-Based Solid Lipid Nanocarriers for Flavonoids Delivery. *Colloids Surf. Physicochem. Eng. Asp.* **2014**, *460*, 483–493. https://doi.org/10.1016/j.colsurfa.2014.02.034.

(68) Wang, C.; Tong, Q.; Hou, X.; Hu, S.; Fang, J.; Sun, C. C. Enhancing Bioavailability of Dihydromyricetin through Inhibiting Precipitation of Soluble Cocrystals by a Crystallization Inhibitor. *Cryst. Growth Des.* **2016**, *16* (9), 5030–5039. https://doi.org/10.1021/acs.cgd.6b00591.

(69) Drozd, K. V.; Manin, A. N.; Churakov, A. V.; Perlovich, G. L. Drug-Drug Cocrystals of Antituberculous 4-Aminosalicylic Acid: Screening, Crystal Structures, Thermochemical and Solubility Studies. *Eur. J. Pharm. Sci.* **2017**, *99*, 228–239. https://doi.org/10.1016/j.ejps.2016.12.016.

(70) Zhu, B.; Zhang, Q.; Wang, J.-R.; Mei, X. Cocrystals of Baicalein with Higher Solubility and Enhanced Bioavailability. *Cryst. Growth Des.* **2017**, *17* (4), 1893–1901. https://doi.org/10.1021/acs.cgd.6b01863.

(71) Putra, O. D.; Umeda, D.; Nugraha, Y. P.; Furuishi, T.; Nagase, H.; Fukuzawa, K.; Uekusa, H.; Yonemochi, E. Solubility Improvement of Epalrestat by Layered Structure Formation via Cocrystallization. *CrystEngComm* **2017**, *19* (19), 2614–2622. https://doi.org/10.1039/C7CE00284J.

(72) Bordignon, S.; Cerreia Vioglio, P.; Priola, E.; Voinovich, D.; Gobetto, R.; Nishiyama, Y.; Chierotti, M. R. Engineering Codrug Solid Forms: Mechanochemical Synthesis of an Indomethacin–Caffeine System. *Cryst. Growth Des.* **2017**, *17* (11), 5744–5752. https://doi.org/10.1021/acs.cgd.7b00748.

(73) Latif, S.; Abbas, N.; Hussain, A.; Arshad, M. S.; Bukhari, N. I.; Afzal, H.; Riffat, S.; Ahmad, Z. Development of Paracetamol-Caffeine Co-Crystals to Improve Compressional, Formulation and *in Vivo* Performance. *Drug Dev. Ind. Pharm.* **2018**, *44* (7), 1099–1108. https://doi.org/10.1080/03639045.2018.1435687.

(74) Aitipamula, S.; Cadden, J.; Chow, P. S. Cocrystals of Zonisamide: Physicochemical Characterization and Sustained Release Solid Forms. *CrystEngComm* **2018**, *20* (21), 2923–2931. https://doi.org/10.1039/C8CE00084K.

(75) do Amaral, L. H.; do Carmo, F. A.; Amaro, M. I.; de Sousa, V. P.; da Silva, L. C. R. P.; de Almeida, G. S.; Rodrigues, C. R.; Healy, A. M.; Cabral, L. M. Development and Characterization of Dapsone Cocrystal Prepared by Scalable Production Methods. *AAPS PharmSciTech* **2018**, *19* (6), 2687–2699. https://doi.org/10.1208/s12249-018-1101-5.

(76) Souza, M. S.; Diniz, L. F.; Vogt, L.; Carvalho, P. S.; D'vries, R. F.; Ellena, J. Avoiding Irreversible 5-Fluorocytosine Hydration *via* Supramolecular Synthesis of Pharmaceutical Cocrystals. *New J. Chem.* **2018**, *42* (18), 14994–15005. https://doi.org/10.1039/C8NJ02647E.

(77) Luo, Y.; Chen, S.; Zhou, J.; Chen, J.; Tian, L.; Gao, W.; Zhang, Y.; Ma, A.; Li, L.; Zhou, Z. Luteolin Cocrystals: Characterization, Evaluation of Solubility, Oral Bioavailability and Theoretical Calculation. *J. Drug Deliv. Sci. Technol.* **2019**, *50*, 248–254. https://doi.org/10.1016/j.jddst.2019.02.004.

(78) Cui, W.; He, Z.; Zhang, Y.; Fan, Q.; Feng, N. Naringenin Cocrystals Prepared by Solution Crystallization Method for Improving Bioavailability and Anti-Hyperlipidemia Effects. *AAPS PharmSciTech* **2019**, *20* (3), 115. https://doi.org/10.1208/s12249-019-1324-0.

(79) Mohite, R.; Mehta, P.; Arulmozhi, S.; Kamble, R.; Pawar, A.; Bothiraja, C. Synthesis of Fisetin Co-Crystals with Caffeine and Nicotinamide Using the Cooling Crystallization Technique: Biopharmaceutical Studies. *New J. Chem.* **2019**, *43* (34), 13471–13479. https://doi.org/10.1039/C9NJ01848D.

(80) Saikia, B.; Sultana, N.; Kaushik, T.; Sarma, B. Engineering a Remedy to Improve Phase Stability of Famotidine under Physiological PH Environments. *Cryst. Growth Des.* **2019**, *19* (11), 6472–6481. https://doi.org/10.1021/acs.cgd.9b00931.
(81) Verdugo-Escamilla, C.; Alarcón-Payer, C.; Frontera, A.; Acebedo-Martínez, F. J.; Domínguez-Martín, A.; Gómez-Morales, J.; Choquesillo-Lazarte, D. Interconvertible Hydrochlorothiazide–Caffeine Multicomponent Pharmaceutical Materials: A Solvent Issue. *Crystals* **2020**, *10* (12), 1088. https://doi.org/10.3390/cryst10121088.
(82) Madan, J. R.; Waghmare, S. V.; Patil, R. B.; Awasthi, R.; Dua, K. Cocrystals of Apixaban with Improved Solubility and Permeability: Formulation, Physicochemical Characterization, Pharmacokinetic Evaluation, and Computational Studies. *ASSAY Drug Dev. Technol.* **2021**, *19* (2), 124–138. https://doi.org/10.1089/adt.2020.1052.
(83) Baptista, J. A.; Castro, R. A. E.; Rosado, M. T. S.; Maria, T. M. R.; Silva, M. R.; Canotilho, J.; Eusébio, M. E. S. Polymorphic Cocrystals of the Antimalarial Drug Pyrimethamine: Two Case Studies. *Cryst. Growth Des.* **2021**, *21* (7), 3699–3713. https://doi.org/10.1021/acs.cgd.1c00005.
(84) Acebedo-Martínez, F. J.; Alarcón-Payer, C.; Frontera, A.; Barbas, R.; Prohens, R.; Di Crisci, M.; Domínguez-Martín, A.; Gómez-Morales, J.; Choquesillo-Lazarte, D. Novel Polymorphic Cocrystals of the Non-Steroidal Anti-Inflammatory Drug Niflumic Acid: Expanding the Pharmaceutical Landscape. *Pharmaceutics* **2021**, *13* (12), 2140. https://doi.org/10.3390/pharmaceutics13122140.
(85) Rodríguez-Ruiz, C.; Montes-Tolentino, P.; Domínguez-Chávez, J. G.; Morales-Rojas, H.; Höpfl, H.; Herrera-Ruiz, D. Tailoring Chlorthalidone Aqueous Solubility by Cocrystallization: Stability and Dissolution Behavior of a Novel Chlorthalidone-Caffeine Cocrystal. *Pharmaceutics* **2022**, *14* (2), 334. https://doi.org/10.3390/pharmaceutics14020334.
(86) Shalmashi, A.; Golmohammad, F. Solubility of Caffeine in Water, Ethyl Acetate, Ethanol, Carbon Tetrachloride, Methanol, Chloroform, Dichloromethane, and Acetone between 298 and 323 K. *Lat. Am. Appl. Res.* **2010**, *40* (3), 283.
(87) Cai, Q.; Xue, J.; Wang, Q.; Du, Y. Investigation into Structure and Dehydration Dynamic of Gallic Acid Monohydrate: A Raman Spectroscopic Study. *Spectrochim. Acta. A. Mol. Biomol. Spectrosc.* **2018**, *201*, 128–133. https://doi.org/10.1016/j.saa.2018.05.002.
(88) Braun, D. E.; Bhardwaj, R. M.; Florence, A. J.; Tocher, D. A.; Price, S. L. Complex Polymorphic System of Gallic Acid—Five Monohydrates, Three Anhydrates, and over 20 Solvates. *Cryst. Growth Des.* **2013**, *13* (1), 19–23. https://doi.org/10.1021/cg301506x.
(89) Gowayed, O. Y.; Moosa, T.; Moratos, A. M.; Hua, T.; Arnold, S.; Garetz, B. A. Dynamic Light Scattering Study of a Laser-Induced Phase-Separated Droplet of Aqueous Glycine. *J. Phys. Chem. B* **2021**, *125* (28), 7828–7839. https://doi.org/10.1021/acs.jpcb.1c02620.
(90) Bérar, J. F.; Calvarin, G.; Weigel, D. Un Goniomètre Original Très Précis Pour La Diffraction Des Rayons X Sur Poudre à Température Controlée. *J. Appl. Crystallogr.* **1980**, *13* (3), 201–206. https://doi.org/10.1107/S0021889880011934.
(91) Boultif, A.; Louër, D. Powder Pattern Indexing with the Dichotomy Method. *J. Appl. Crystallogr.* **2004**, *37* (5), 724–731. https://doi.org/10.1107/S0021889804014876.
(92) Rodriguez-Carvajal, J.; Roisnel, T. FullProf.98 and WinPLOTR: New Windows 95/NT Applications for Diffraction Commission For Powder Diffraction, 1998.

(93) Edwards, H. G. M.; Munshi, T.; Anstis, M. Raman Spectroscopic Characterisations and Analytical Discrimination between Caffeine and Demethylated Analogues of Pharmaceutical Relevance. *Spectrochim. Acta. A. Mol. Biomol. Spectrosc.* **2005**, *61* (7), 1453–1459. https://doi.org/10.1016/j.saa.2004.10.022.
(94) Pompeu, D. R.; Larondelle, Y.; Rogez, H.; Abbas, O.; Pierna, J. A. F.; Baeten, V. Characterization and discrimination of phenolic compounds using Fourier transform Raman spectroscopy and chemometric tools. *BASE* **2018**, 13–28. https://doi.org/10.25518/1780-4507.16270.
(95) Mohammed-Ziegler, I.; Billes, F. Vibrational Spectroscopic Calculations on Pyrogallol and Gallic Acid. *J. Mol. Struct. THEOCHEM* **2002**, *618* (3), 259–265. https://doi.org/10.1016/S0166-1280(02)00547-X.
(96) Good, D. J.; Rodríguez-Hornedo, N. Solubility Advantage of Pharmaceutical Cocrystals. *Cryst. Growth Des.* **2009**, *9* (5), 2252–2264. https://doi.org/10.1021/cg801039j.

Tables and figures captions

Table 1. Pertinent values of the DSC and TG curves for the CAF and GAL cocrystals and comparison with the literature.

Table 2. Cell parameters of different CAF and GAL cocrystals.

Scheme 1. Crystallization methods, internal code name, chemical formula, behavior in temperature.

Figure 1. Photography of cocrystals a) Vial of 1.5 ml. Cocrystals of CAF-GAL_NPLIN_296 are visible at the interface where nucleation occurs and fall at the bottom. b) Bottom of the vials before laser irradiation. c) Bottom of the vials 3 hours after laser irradiation. The cocrystals shadows nucleated at the meniscus are visible. d) Very fine needles in solution which have fallen at the bottom 48 h after irradiation. e) Appearance of the cocrystals of CAF-GAL_NPLIN_296 after filtration. The fine needles are glued to aggregates. f) Appearance of the cocrystals aggregates of CAF-GAL_SN_296 after filtration.

Figure 2. Probability of nucleation of CAF-GAL_NPLIN_296 at 296 K as a function of molarity, laser exposition: 100 pulses; CAF caffeine, GAL gallic acid. Probability of nucleation is determined on the day of the experiment (Day 0) or two days later (Day +2).

Figure 3. Raman. a) Comparison of CAF-GAL_NPLIN_296 and CAF-GAL_SN_296 with the initial product spectra. Insert zoom at low wavenumbers depicting the lattice vibration. b) Low wavenumbers of CAF-GAL_NPLIN_296, CAF-GAL_SN_A_296, CAF-GAL_SN_B_296 (bold line) and their anhydride forms (fine line).

Figure 4. TG/DSC curves for cocrystals a) CAF-GAL_SN_A_296 b) CAF-GAL_SN_ A_353 c) CAF-GAL_NPLIN_296.

Figure 5. PXRD diffractogram of cocrystals obtained in this work, compared to those published in the literature CAF-GAL_Clarke_100, CAF-GAL_Clarke_298, CAF-GAL_Clarke_373 [41]; CAF-GAL_Syed_373 [42], CAF-GAL_Dabir_373 [43] . Each spectrum is represented on its own scale.

Figure 6. PXRD diffractogram of cocrystals as a function of the temperature. Peaks are colored according to their intensities; a) starting material CAF-GAL_SN_A_296; b) starting material CAF-GAL_NPLIN_296; c) T = 400 K. Comparison of the anhydrous cocrystals obtained by heating on the X-ray diffractometer of CAF-GAL_SN_A_296 at 400 K labeled CAF-GAL_SN_A_400 and of CAF-GAL_NPLIN_296 at 400 K labeled CAF-GAL_NPLIN_400.

Table 1. *Pertinent values of the DSC, TG, and PXRD spectra for the CAF and GAL cocrystals and comparison with the literature.*

	Transition temperature (K)		2nd event (K)		Percentage loss of water (%)	Temperature of the loss of water TG (K)	Melting point (K)			Reference
	DSC	PXRD	DSC	PXRD	TG	TG	DSC	TG	PXRD	
CAF-GAL_SN_A_296	357	315	449.7	450	2.37	356	510.5	509.5	510	
CAF-GAL_SN_ A_353	-	-	-	-	-	-	511	511	-	
CAF-GAL_NPLIN_296	317.5	318		460-480	7.91	316.5	495,6	509	490	
CAF-GAL_Clarke_296	409				1.9		514			[41]
CAF-GAL_Clarke_373							516			[41]
CAF-GAL_Syed_373							519			[42]
CAF-GAL_Dabir_373							514			[43]

Table 2. Cell parameters of the different CAF and GAL cocrystals.

		T(K)	a(Å)	b(Å)	c(Å)	β(°)	V(Å^3)	χ^2
CAF-GAL_Clarck_100	**CAF-GAL.0.5H$_2$O** form I [41]	100	19.966(4)	15.800(3)	13.111(3)	130.780(3)	3131.8(11)	-
	3CAF-GAL.6H$_2$O [44]	150	16.5434(3)	6.79456(11)	18.1390(4)	110.865(2)	1905.21(7)	-
CAF-GAL_SN_A_296	**CAF-GAL.0.5H$_2$O** form II (this work)	296	11.943(6)	12.436(4)	9.778(3)	104.5(3)	1405.6(9)	6.61
CAF-GAL_SN_A_353	**CAF-GAL.0.5H$_2$O** (this work)	296	23.449(8)	11.732(4)	8.530(3)	91.6(1)	2342.9(1)	9.25

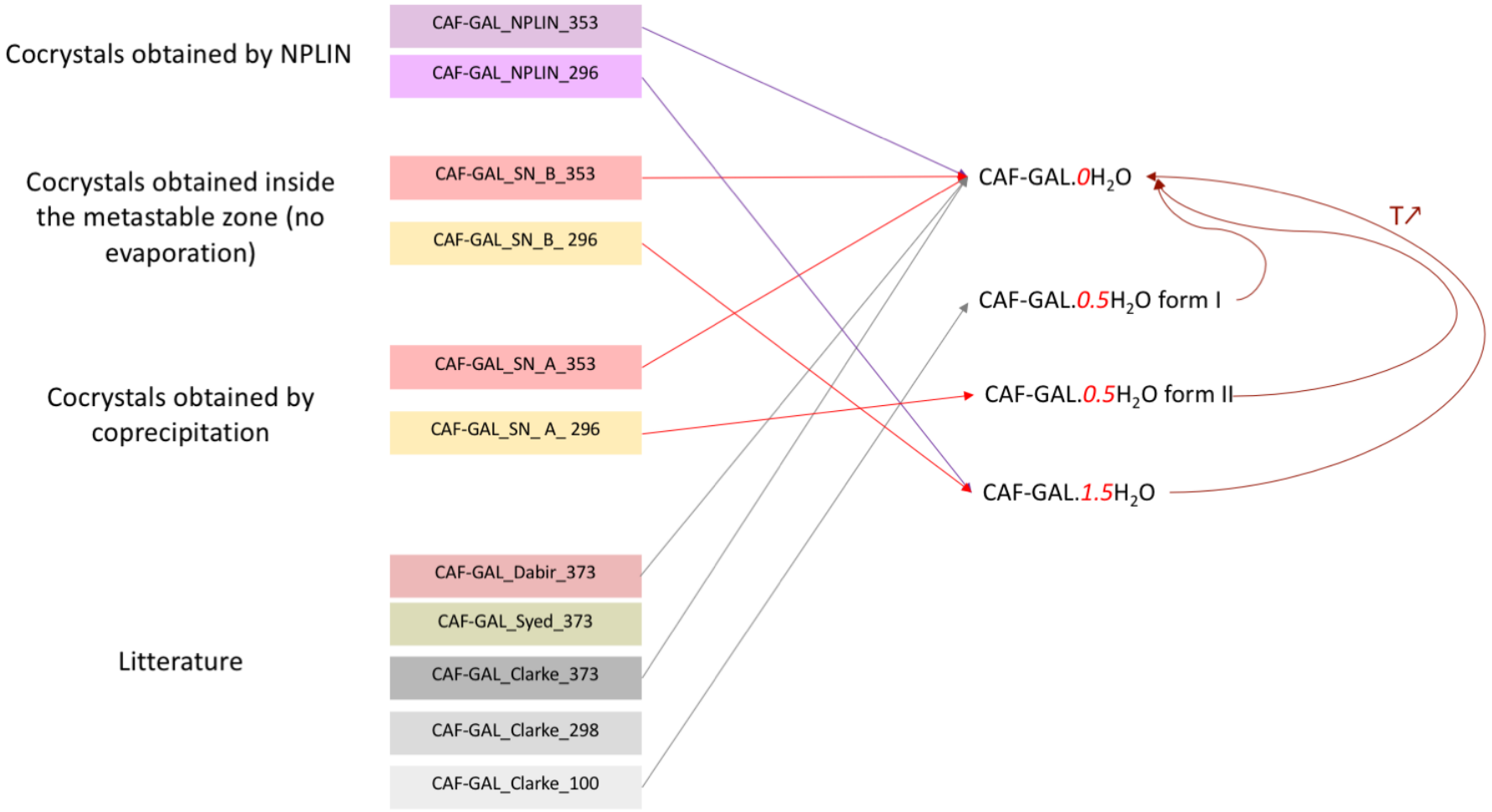
Cocrystals obtained by NPLIN
CAF-GAL_NPLIN_353
CAF-GAL_NPLIN_296
Cocrystals obtained inside the metastable zone (no evaporation)
CAF-GAL_SN_B_353
CAF-GAL_SN_B_ 296
Cocrystals obtained by coprecipitation
CAF-GAL_SN_A_353
CAF-GAL_SN_ A_ 296
Litterature
CAF-GAL_Dabir_373
CAF-GAL_Syed_373
CAF-GAL_Clarke_373
CAF-GAL_Clarke_298
CAF-GAL_Clarke_100
CAF-GAL.0H2O
CAF-GAL.0.5H2O form I
CAF-GAL.0.5H2O form II
CAF-GAL.1.5H2O
T↗

Scheme 1

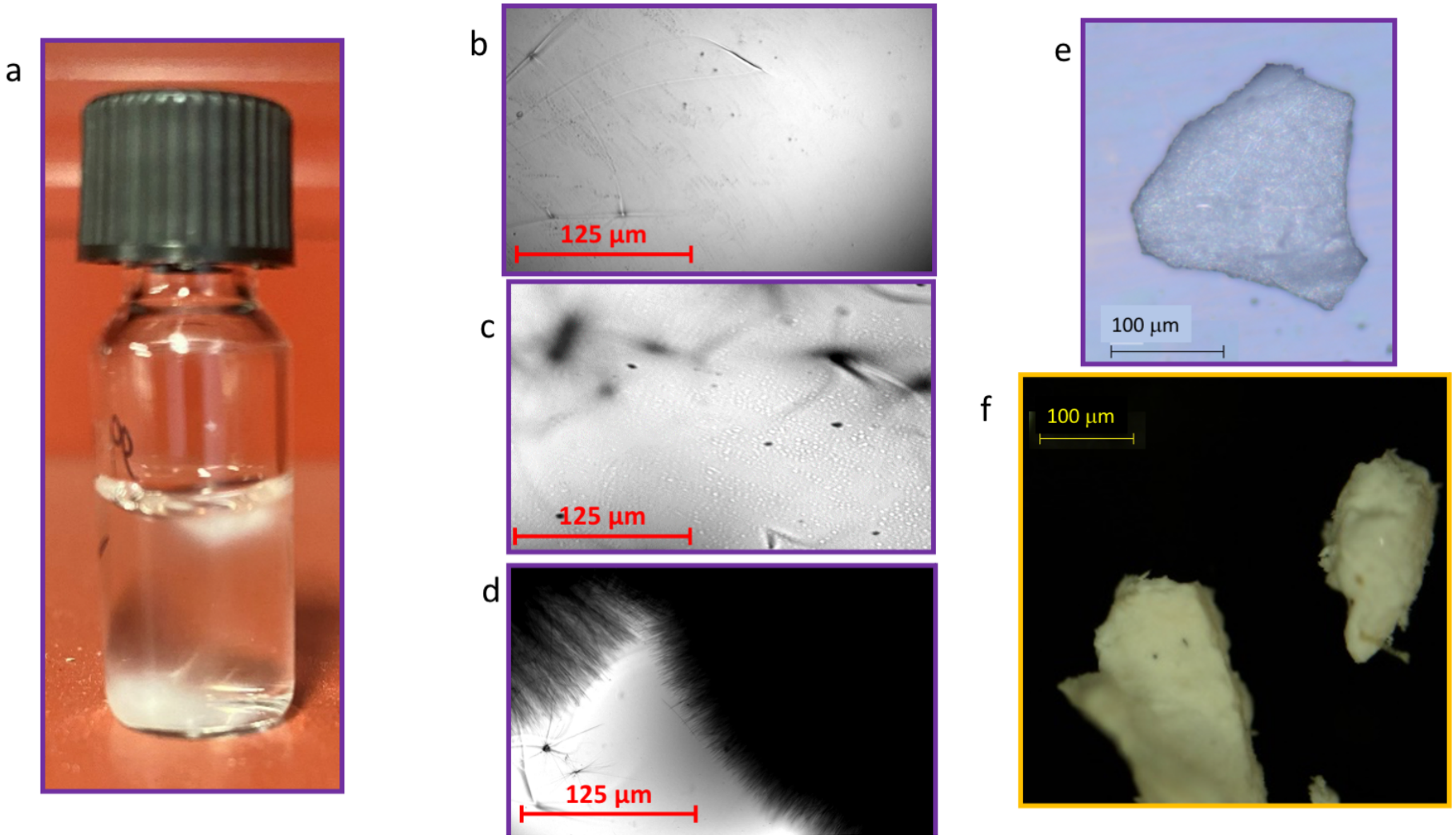

Figure 1

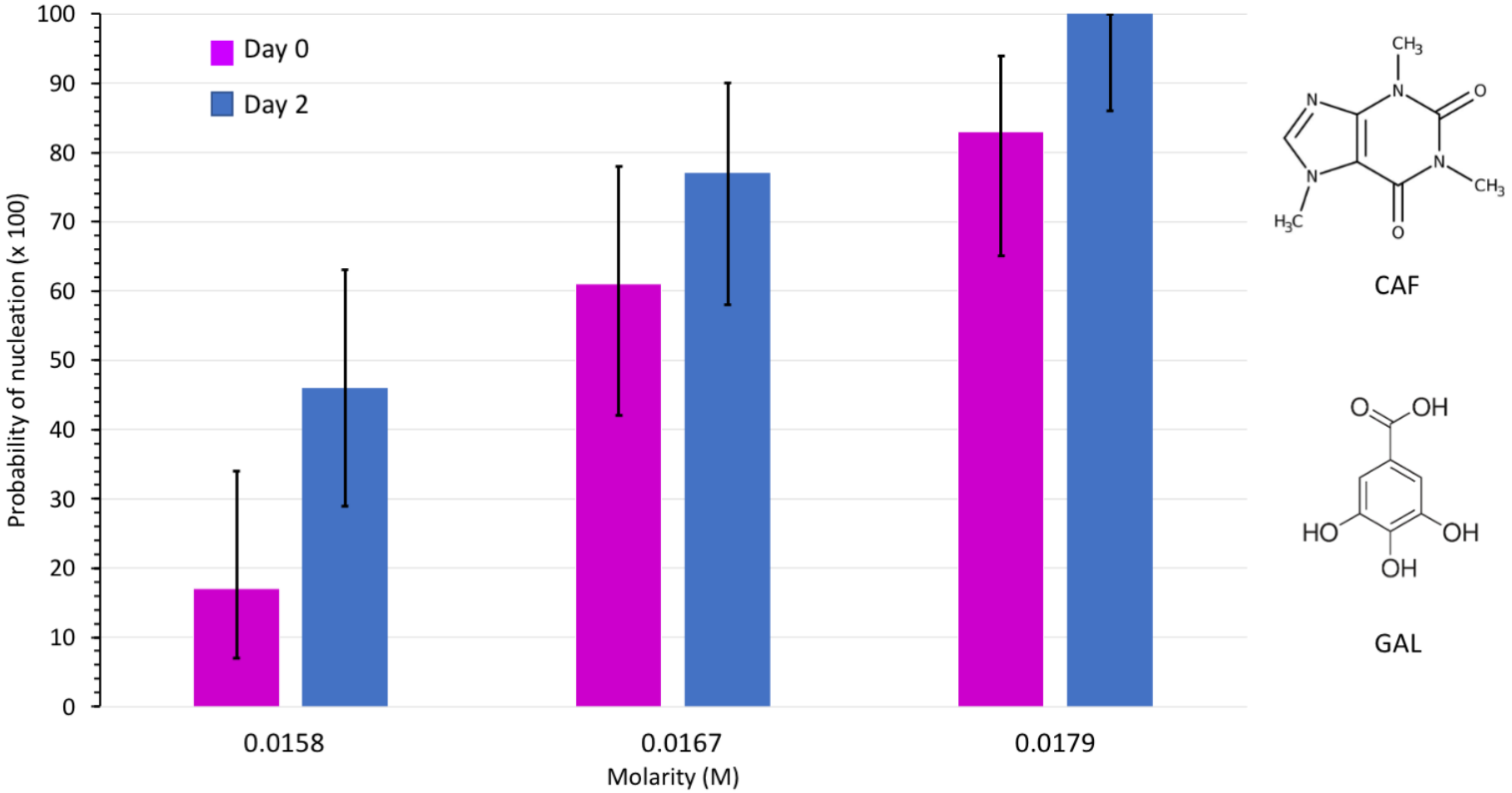
Day 0
Day 2
Probability of nucleation (x 100)
100
90
80
70
60
50
40
30
20
10
0
0.0158
0.0167
0.0179
Molarity (M)
CAF
GAL

Figure 2

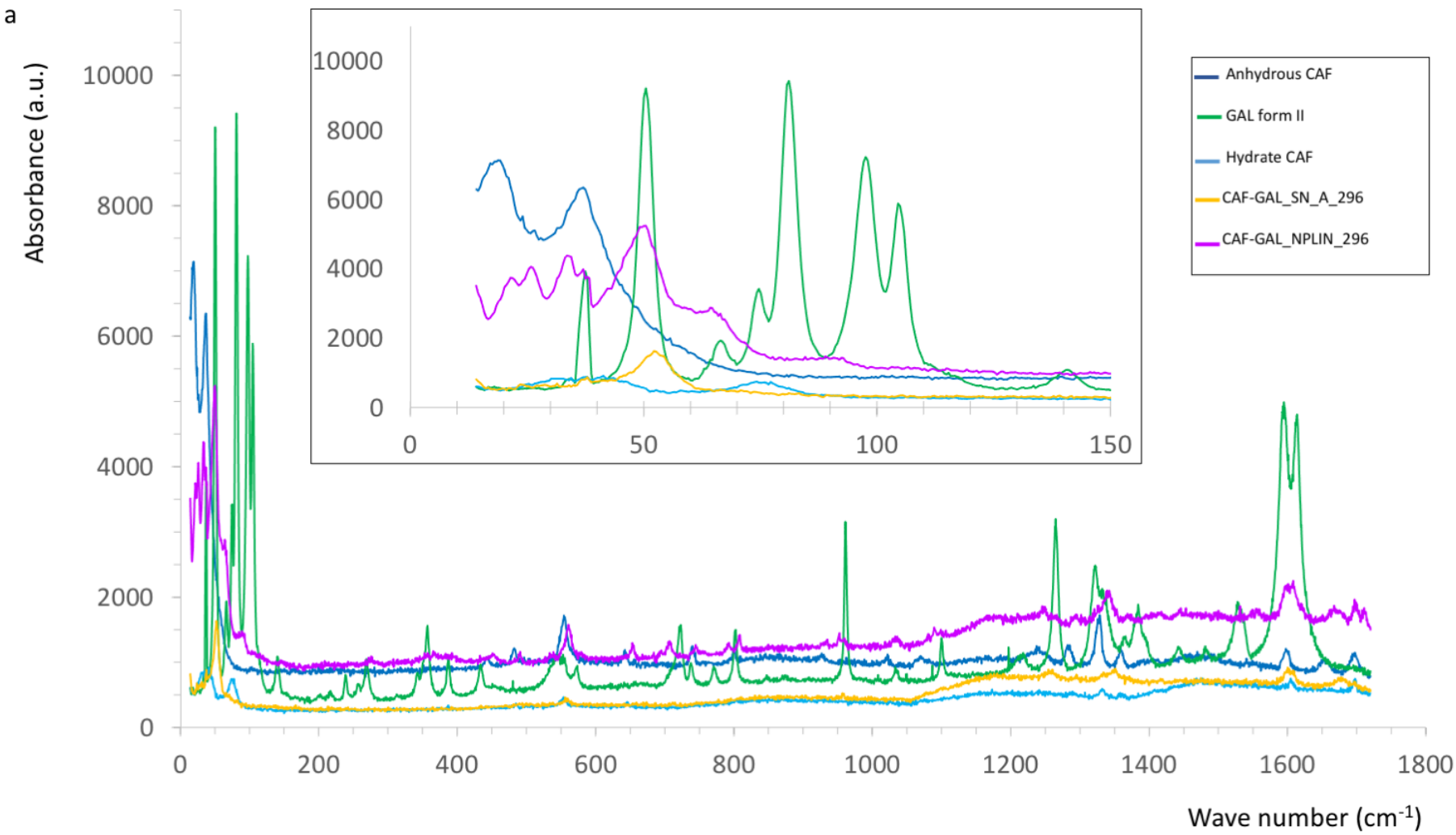
a
Absorbance (a.u.)
10000
8000
6000
4000
2000
0
0
200
400
600
800
1000
1200
1400
1600
1800
Wave number (cm-1)
10000
8000
6000
4000
2000
0
0
50
100
150
Anhydrous CAF
GAL form II
Hydrate CAF
CAF-GAL_SN_A_296
CAF-GAL_NPLIN_296

Figure 3a

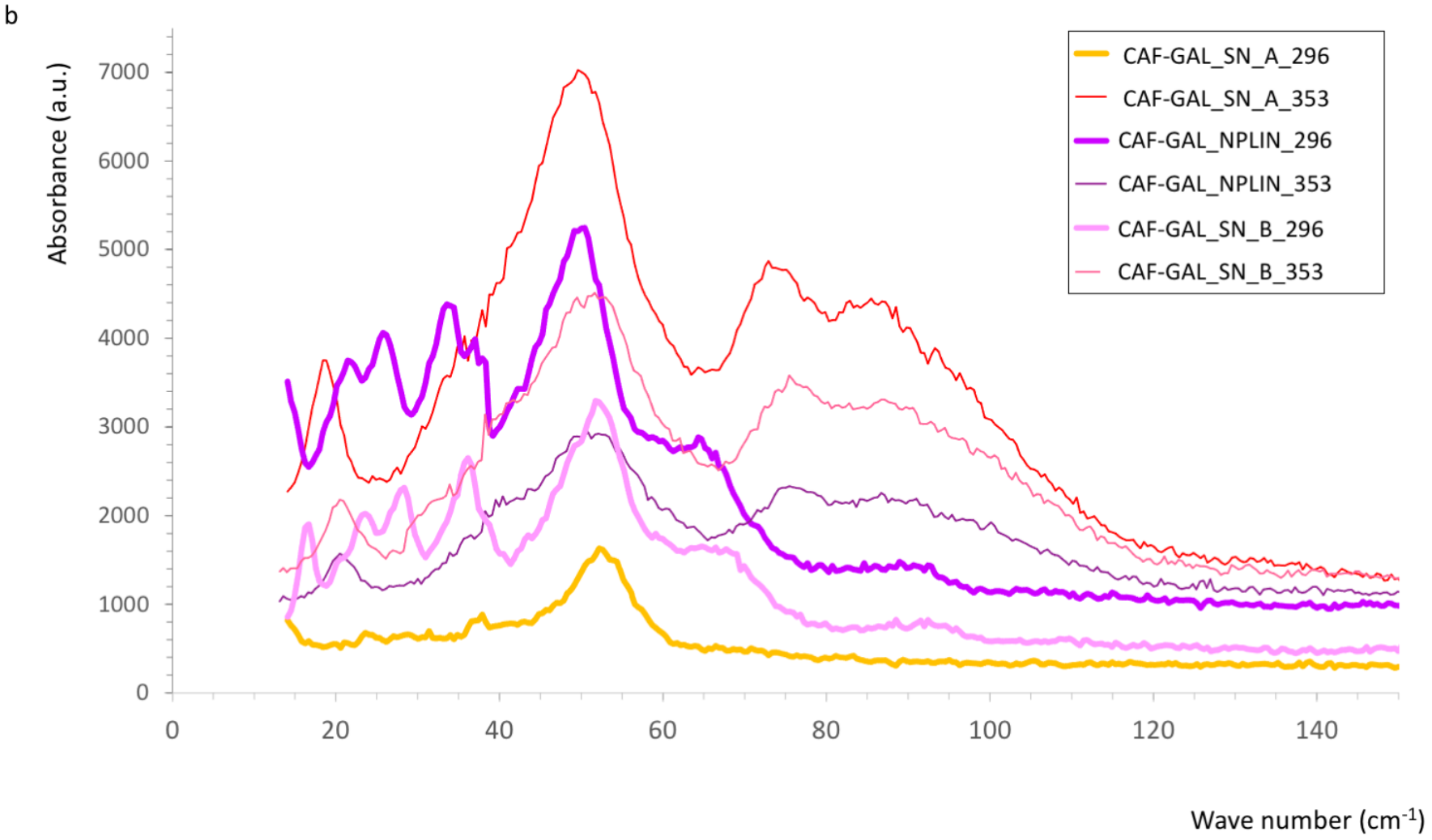
b
Absorbance (a.u.)
7000
6000
5000
4000
3000
2000
1000
0
0
20
40
60
80
100
120
140
Wave number (cm-1)
CAF-GAL_SN_A_296
CAF-GAL_SN_A_353
CAF-GAL_NPLIN_296
CAF-GAL_NPLIN_353
CAF-GAL_SN_B_296
CAF-GAL_SN_B_353

Figure 3b

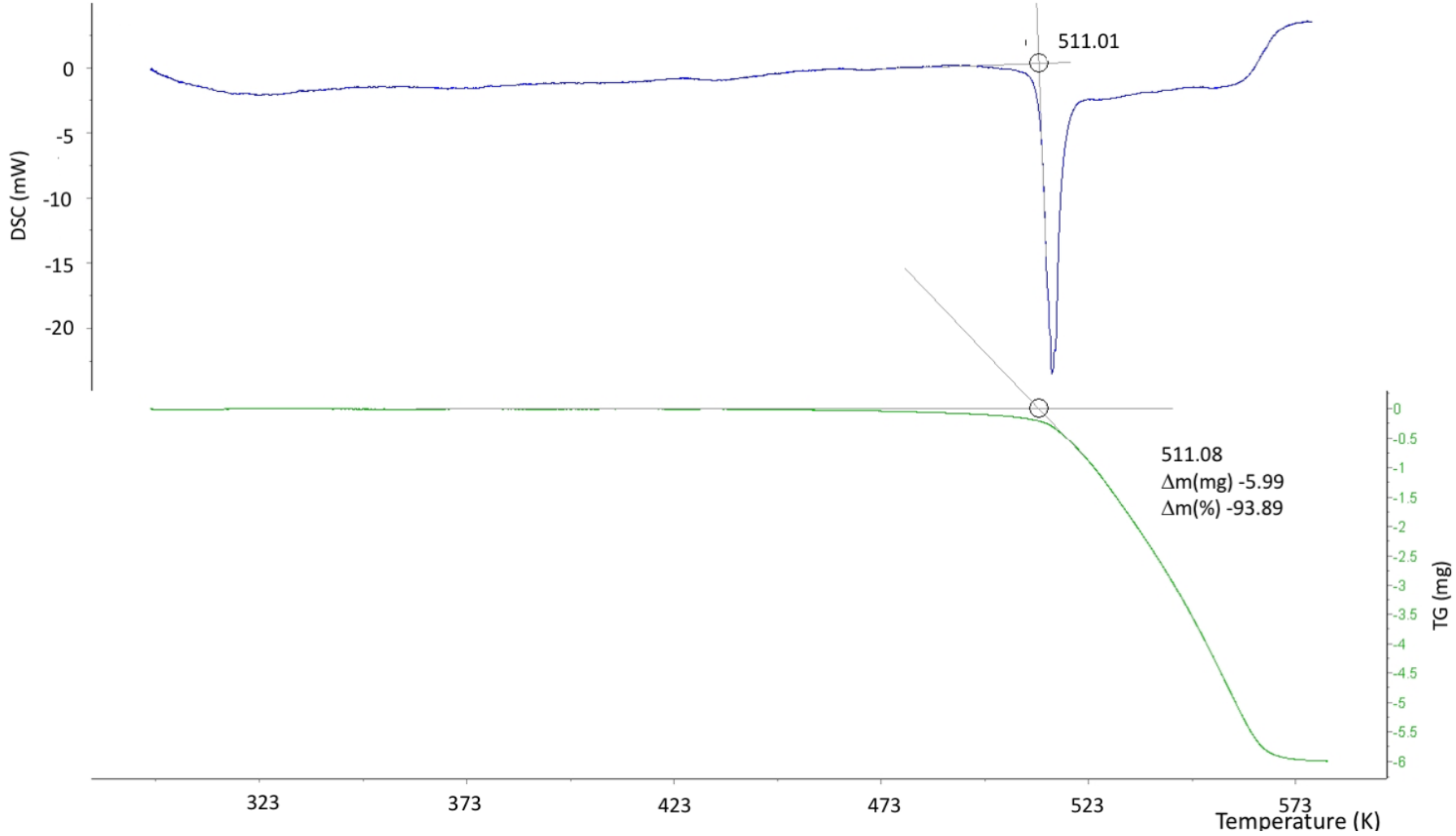
511.01
511.08
Δm(mg) -5.99
Δm(%) -93.89
DSC (mW)
TG (mg)
Temperature (K)
0
-5
-10
-15
-20
323
373
423
473
523
573
-0.5
-1
-1.5
-2
-2.5
-3
-3.5
-4
-4.5
-5
-5.5
-6

Figure 5a

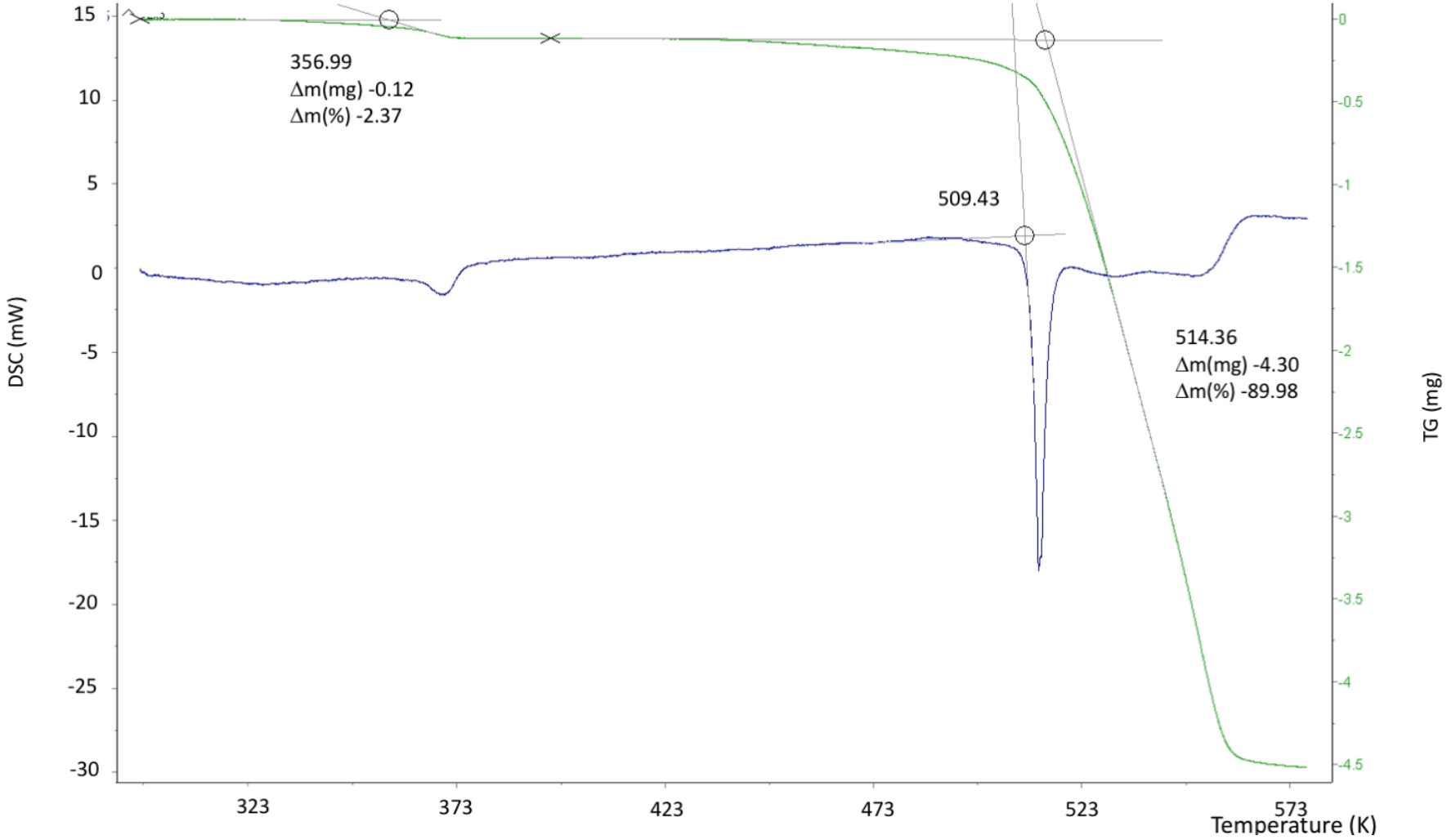
356.99
Δm(mg) -0.12
Δm(%) -2.37
509.43
514.36
Δm(mg) -4.30
Δm(%) -89.98
DSC (mW)
TG (mg)
Temperature (K)
15
10
5
0
-5
-10
-15
-20
-25
-30
0
-0.5
-1
-1.5
-2
-2.5
-3
-3.5
-4
-4.5
323
373
423
473
523
573

Figure 5b

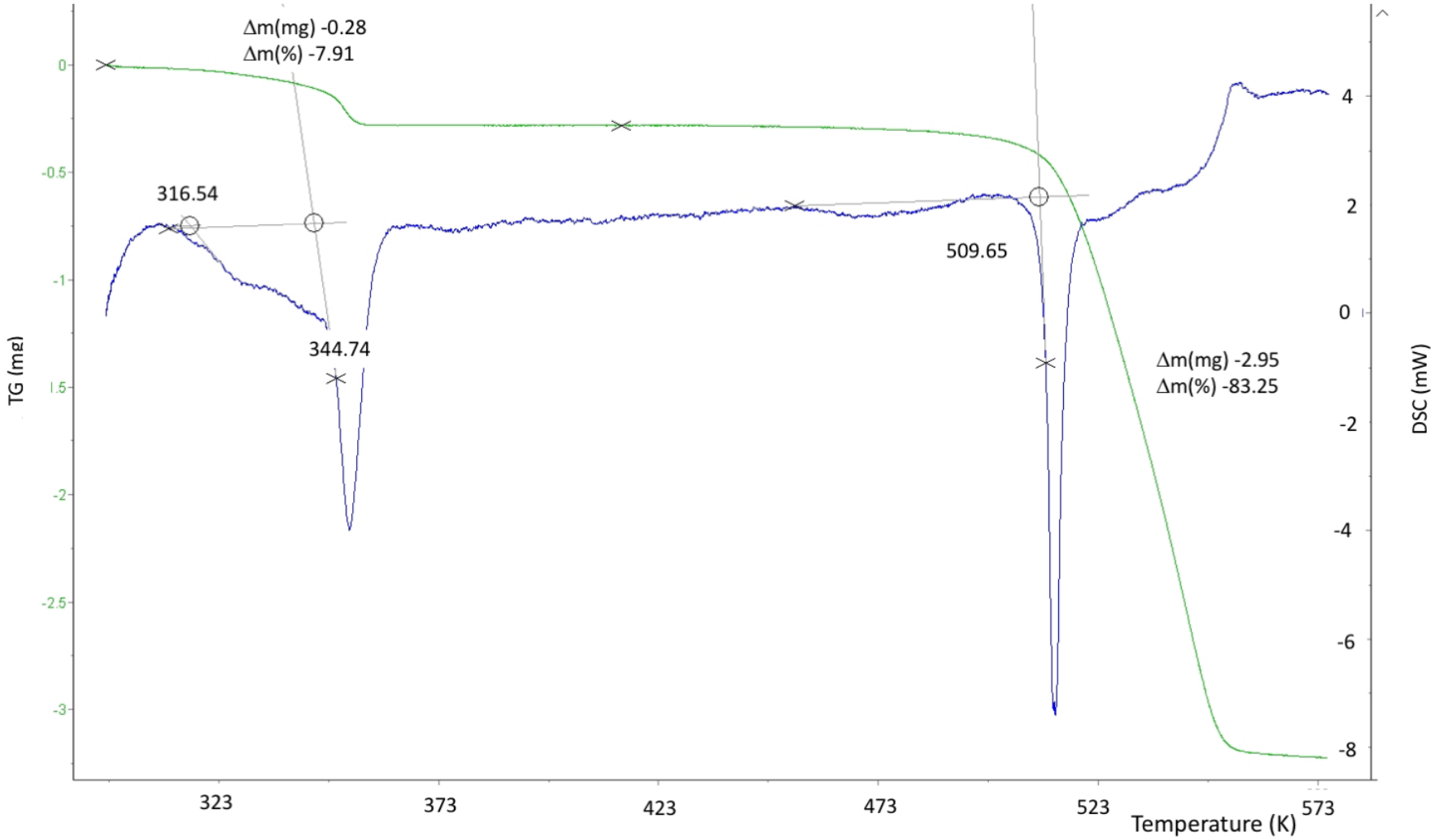
Δm(mg) -0.28
Δm(%) -7.91
316.54
344.74
509.65
Δm(mg) -2.95
Δm(%) -83.25
TG (mg)
DSC (mW)
Temperature (K)
0
-0.5
-1
-1.5
-2
-2.5
-3
4
2
0
-2
-4
-6
-8
323
373
423
473
523
573

Figure 5c

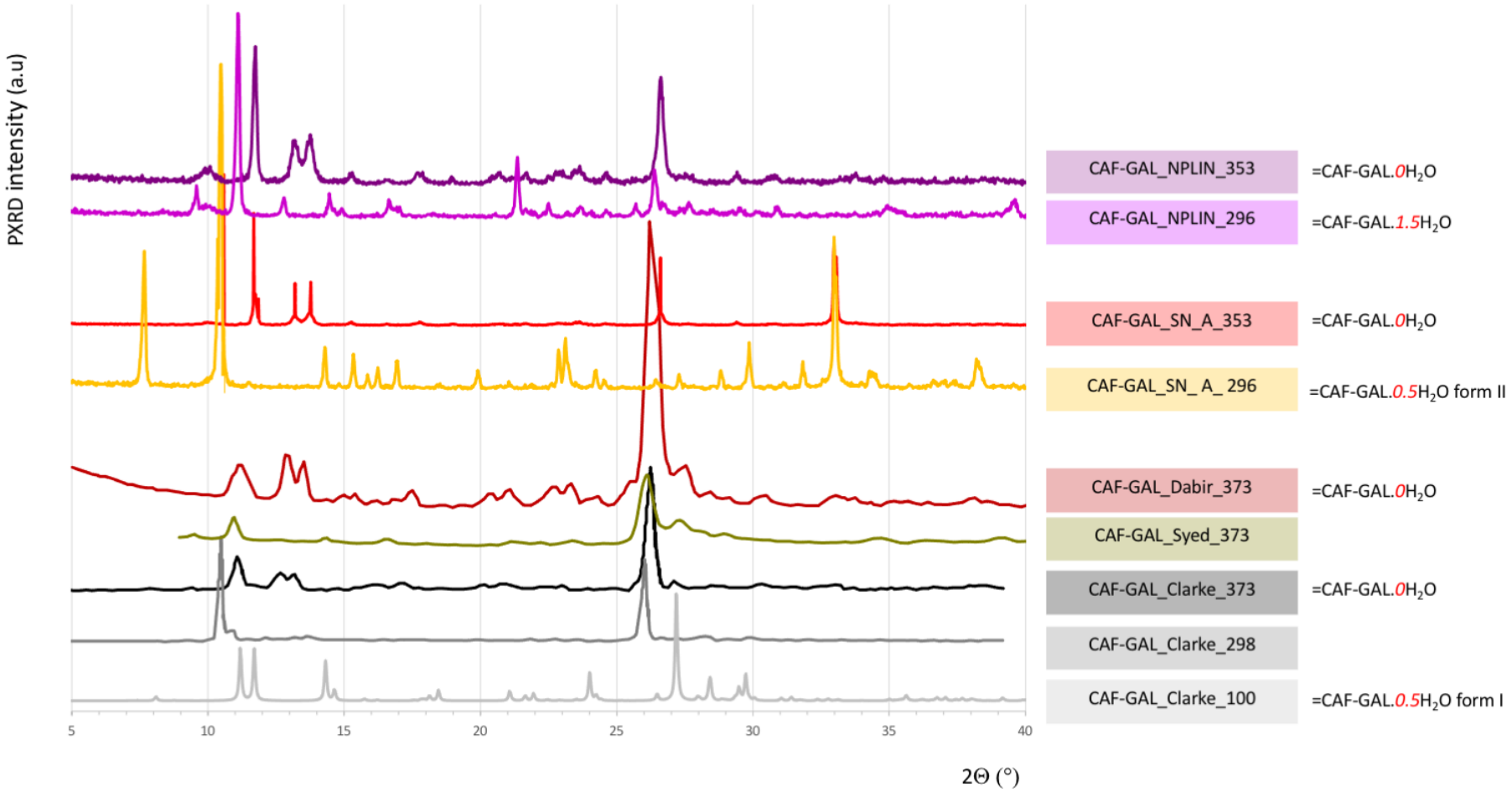
PXRD intensity (a.u)
5
10
15
20
25
30
35
40
2Θ (°)
CAF-GAL_NPLIN_353
=CAF-GAL.0H2O
CAF-GAL_NPLIN_296
=CAF-GAL.1.5H2O
CAF-GAL_SN_A_353
=CAF-GAL.0H2O
CAF-GAL_SN_ A_ 296
=CAF-GAL.0.5H2O form II
CAF-GAL_Dabir_373
=CAF-GAL.0H2O
CAF-GAL_Syed_373
CAF-GAL_Clarke_373
=CAF-GAL.0H2O
CAF-GAL_Clarke_298
CAF-GAL_Clarke_100
=CAF-GAL.0.5H2O form I

Figure 4

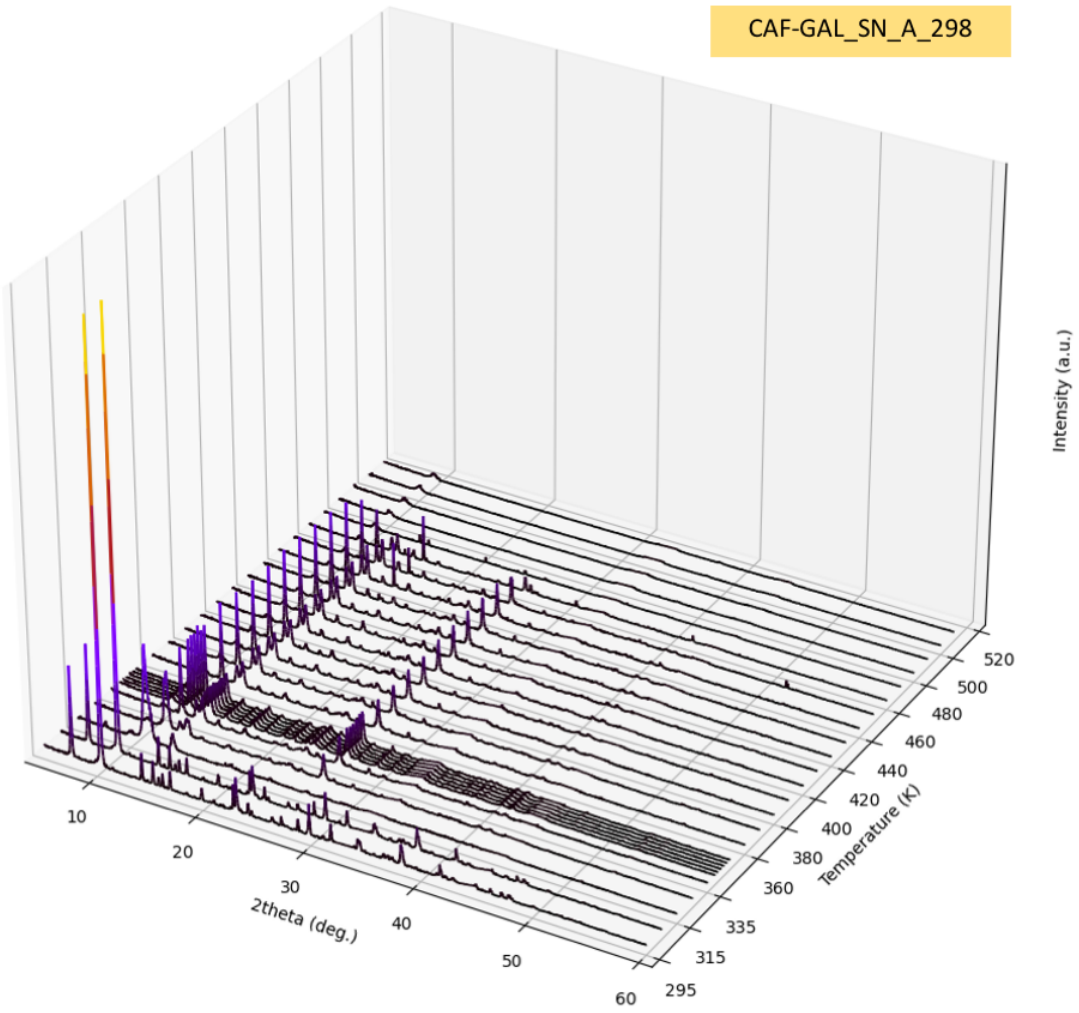
CAF-GAL_SN_A_298
Intensity (a.u.)
Temperature (K)
520
500
480
460
440
420
400
380
360
335
315
295
2theta (deg.)
10
20
30
40
50
60

Figure 6a

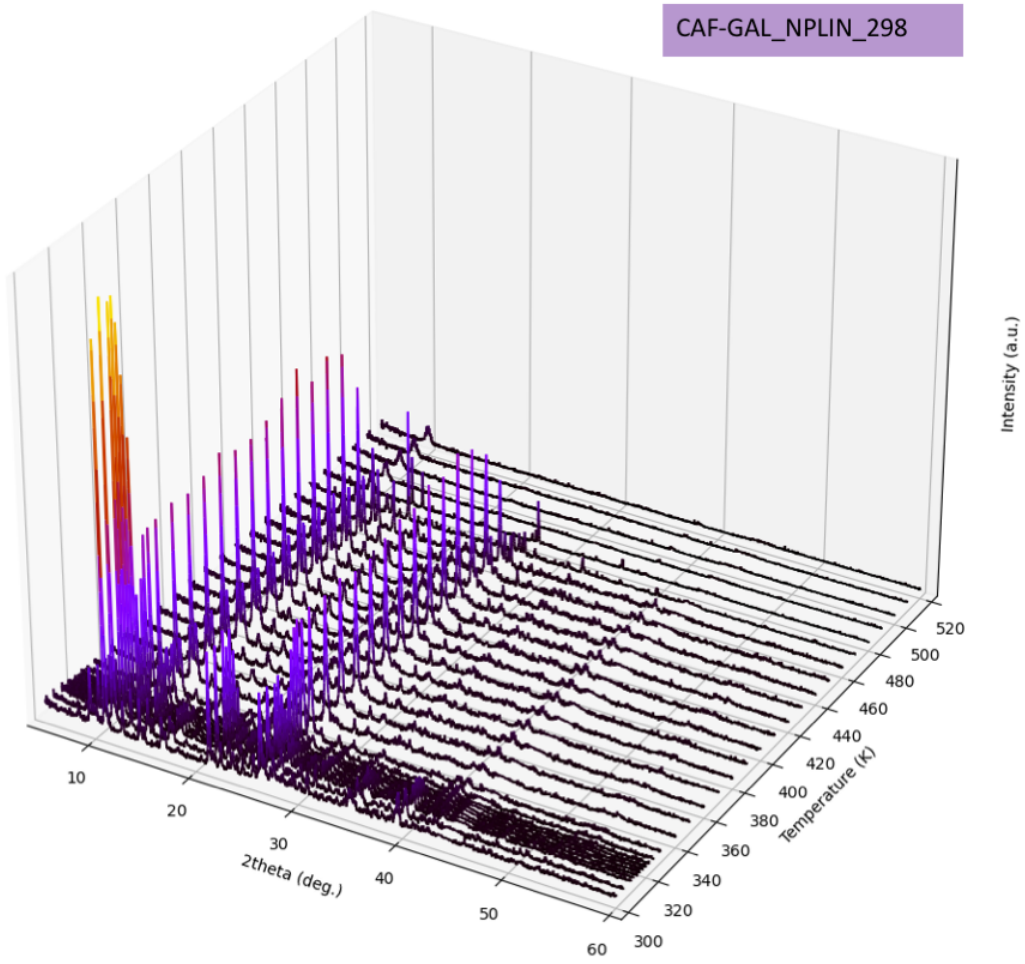
CAF-GAL_NPLIN_298
Intensity (a.u.)
Temperature (K)
520
500
480
460
440
420
400
380
360
340
320
300
2theta (deg.)
10
20
30
40
50
60

Figure 6b

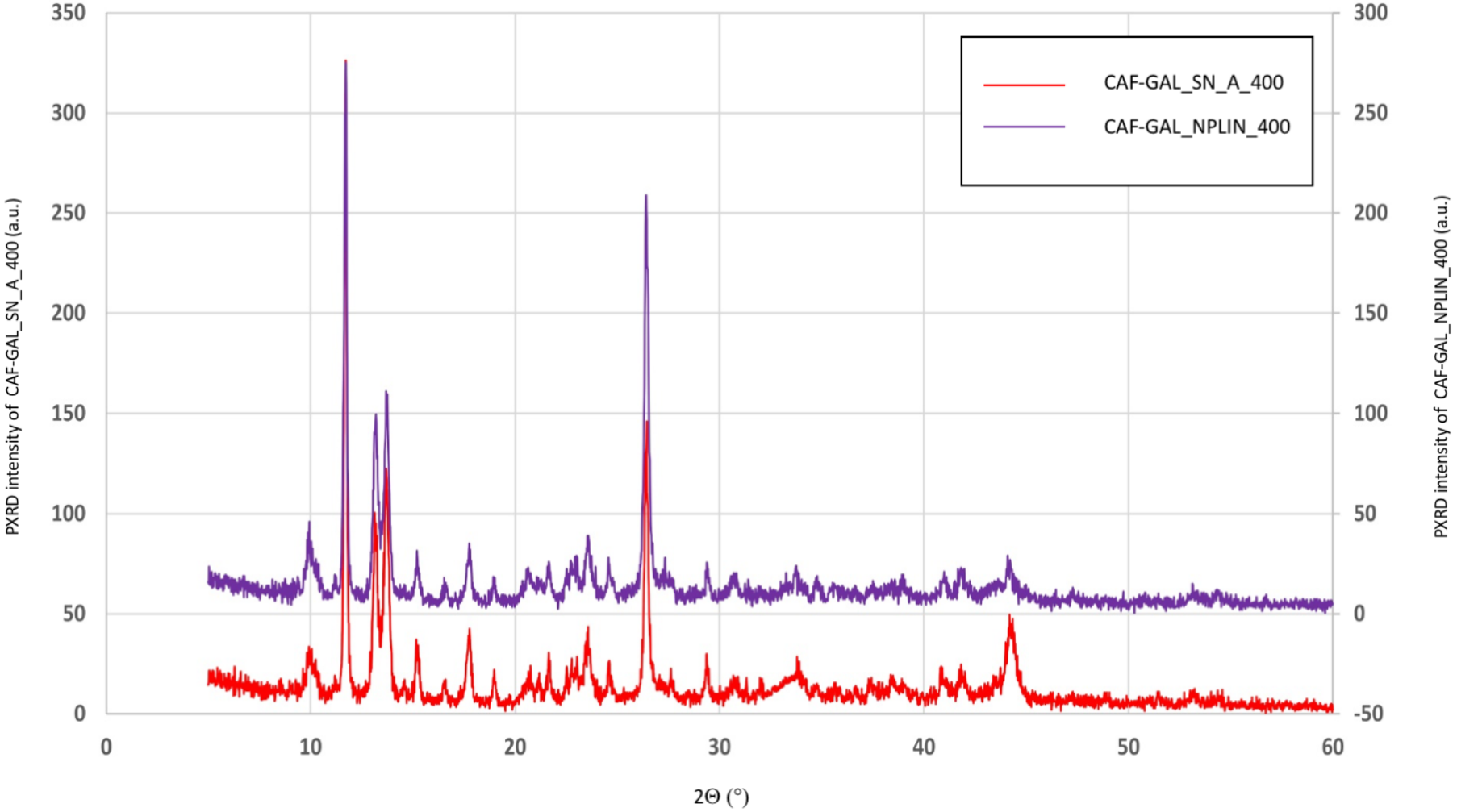
CAF-GAL_SN_A_400
CAF-GAL_NPLIN_400
PXRD intensity of CAF-GAL_SN_A_400 (a.u.)
PXRD intensity of CAF-GAL_NPLIN_400 (a.u.)
2Θ (°)
0
10
20
30
40
50
60
350
300
250
200
150
100
50
0
300
250
200
150
100
50
0
-50

Figure 6c

For Table of Contents Use Only

A new cocrystallization method: Non-Photochemical Laser-Induced Nucleation (NPLIN) of a cocrystal of caffeine–gallic acid in water

Dania MELLAH, Béatrice NICOLAÏ, Bertrand FOURNIER, Nada BOSNJAKOVIC-PAVLOVIC, Francois-Xavier LEGRAND, Pascale GEMEINER, Vincent BOEMARE, Nicolas GUIBLIN, Ali ASSI, Ali TFAYLI, Sokona KONATE, Pierrick DURAND, Anne SPASOJEVIC-de BIRÉ*

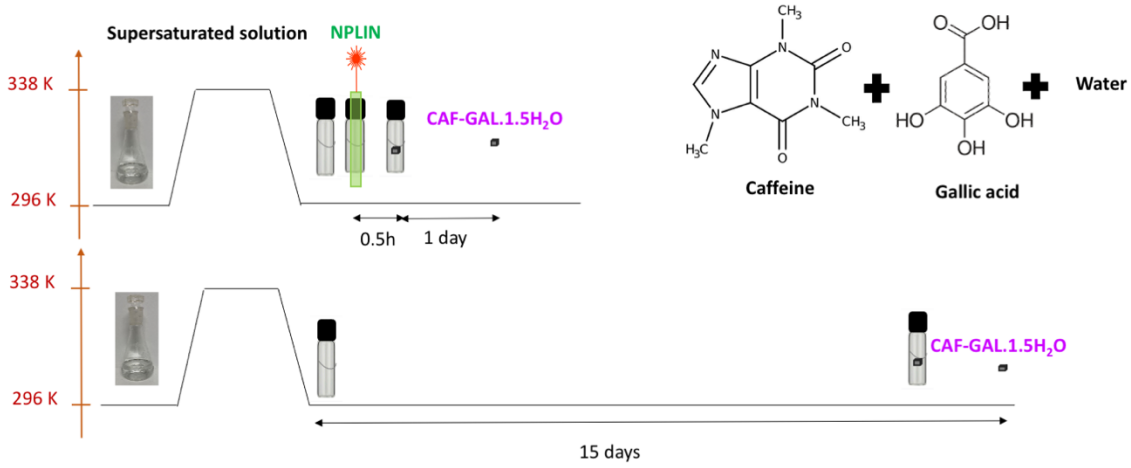

For the first time, cocrystallization of caffeine and gallic acid in water using NPLIN is reported. Induction time is 70 times shorter than spontaneous nucleation. NPLIN allows the obtention of cocrystals *on-demand*, with excellent repeatability. Two new different cocrystal forms are obtained: **CAFGAL.0.5H$_2$O** form II from coprecipitation and **CAFGAL.1.5H$_2$O** from NPLIN and nucleation of a supersaturated solution without evaporation.